

UCLA

UCLA Previously Published Works

Title

Trafficking of mitochondrial double-stranded RNA from mitochondria to the cytosol.

Permalink

<https://escholarship.org/uc/item/8473m5w8>

Journal

Life Science Alliance, 7(9)

Authors

Krieger, Matthew
Abrahamian, Melania
He, Kevin
[et al.](#)

Publication Date

2024-09-01







DOI

10.26508/lsa.202302396

Peer reviewed



Trafficking of mitochondrial double-stranded RNA from mitochondria to the cytosol

Matthew R Krieger¹ , Melania Abrahamian¹, Kevin L He¹ , Sean Atamdede¹, Hesamedin Hakimjavadi², Milica Momcilovic^{3,4}, Dejerianne Ostrow² , Simran DS Maggo², Yik Pui Tsang¹, Xiaowu Gai^{2,5}, Guillaume F Chanfreau^{1,6} , David B Shackelford^{3,4}, Michael A Teitell^{1,4,6,7,8,9} , Carla M Koehler^{1,4,6} 

In addition to mitochondrial DNA, mitochondrial double-stranded RNA (mtdsRNA) is exported from mitochondria. However, specific channels for RNA transport have not been demonstrated. Here, we begin to characterize channel candidates for mtdsRNA export from the mitochondrial matrix to the cytosol. Down-regulation of SUV3 resulted in the accumulation of mtdsRNAs in the matrix, whereas down-regulation of PNPase resulted in the export of mtdsRNAs to the cytosol. Targeting experiments show that PNPase functions in both the intermembrane space and matrix. Strand-specific sequencing of the double-stranded RNA confirms the mitochondrial origin. Inhibiting or down-regulating outer membrane proteins VDAC1/2 and BAK/BAX or inner membrane proteins PHB1/2 strongly attenuated the export of mtdsRNAs to the cytosol. The cytosolic mtdsRNAs subsequently localized to large granules containing the stress protein TIA-1 and activated the type 1 interferon stress response pathway. Abundant mtdsRNAs were detected in a subset of non-small-cell lung cancer cell lines that were glycolytic, indicating relevance in cancer biology. Thus, we propose that mtdsRNA is a new damage-associated molecular pattern that is exported from mitochondria in a regulated manner.

DOI 10.26508/lsa.202302396 | Received 26 September 2023 | Revised 25 June 2024 | Accepted 25 June 2024 | Published online 2 July 2024

Introduction

Whereas the vast majority of mitochondrial proteins are encoded within the nucleus and imported into mitochondria by mechanisms studied in great detail (Chacinska et al, 2009; Becker et al, 2019), less is known about the transport of nucleic acids across the mitochondrial membranes. Nucleic acids that are transported include mitochondrial DNA (mtDNA), nuclear-encoded tRNAs and non-coding RNAs, mitochondrial double-stranded RNAs (mtdsRNA), and viral RNAs. Thus, a

large cohort of nucleic acids cross the mitochondrial outer and inner membranes. Cytosolic mtDNA and recently identified mtdsRNA function as damage-associated molecular patterns (DAMPs) to signal mitochondrial stress (Dhir et al, 2018; Wu et al, 2021) to the rest of the cell.

mtDNA is released from mitochondria as an endogenous trigger for inflammation, activating pro-inflammatory and type 1 IFN (IFN-1) responses (West & Shadel, 2017). The specific manner of release is not known, but potential mechanisms include mitochondrial fragmentation (West et al, 2015), mitophagy (Zhong et al, 2016), apoptosis with mitochondrial herniation (Rongvaux et al, 2014; White et al, 2014; McArthur et al, 2018), and the membrane permeability transition pore (Garcia & Chavez, 2007; Xian et al, 2022), among others. To date, a specific channel for the direct export of mtDNA has not been demonstrated experimentally (West & Shadel, 2017), but recent studies suggest that VDAC and BAK/BAX oligomers with the mitochondrial permeability transition pore may facilitate mtDNA export (Kim et al, 2019; Yu et al, 2020; Xian et al, 2022).

Viral RNAs also translocate into mitochondria, but the specific pathways are not known. Human cytomegalovirus has a 2.7-kilobase RNA, the β 2.7 transcript, that is imported into mitochondria and interacts with complex I to regulate apoptosis (Reeves et al, 2007). The HIV-1 RNA transcripts reside in mitochondria, potentially to compromise mitochondrial function (Somasundaran et al, 1994). Interestingly, computational methods for RNA localization predict that the SARS-CoV-2 RNA genome and subgenomic transcripts (sgRNA) are enriched in the mitochondrial matrix and the nucleolus (Wu et al, 2020). In contrast, these computational methods indicated that transcripts from other SARS viruses did not reside in the mitochondrial matrix. Although these computational predictions have not been verified, support for viral RNA import into mitochondria is warranted as the mitochondria are a critical target in viral replication and propagation strategies.

A variety of cellular RNAs are imported into mitochondria (Sieber et al, 2011; Wang et al, 2012a; Jeandard et al, 2019). Every organism imports at least one nuclear-encoded tRNA, in some cases, that is

¹Department of Chemistry and Biochemistry, UCLA, Los Angeles, CA, USA ²Department of Pathology, Children's Hospital Los Angeles, Los Angeles, CA, USA ³Pulmonary and Critical Care Medicine, David Geffen School of Medicine, UCLA, Los Angeles, CA, USA ⁴Jonsson Comprehensive Cancer Center, UCLA, Los Angeles, CA, USA ⁵Department of Pathology, Keck School of Medicine, University of Southern California, Los Angeles, CA, USA ⁶Molecular Biology Institute, UCLA, Los Angeles, CA, USA ⁷Department of Pathology and Laboratory Medicine, UCLA, Los Angeles, CA, USA ⁸Broad Stem Cell Research Center, UCLA, Los Angeles, CA, USA ⁹NanoSystems Institute, UCLA, Los Angeles, CA, USA

Correspondence: koehlerc@chem.ucla.edu

only required during stress (Simpson & Shaw, 1989; Hancock & Hajduk, 1990; Rubio et al, 2008; Kamenski et al, 2010). Structural RNAs that are imported include the 5S rRNA, H1 RNA of RNase P, and RNase MRP RNA component that are potentially involved in RNA processing and translation in the mitochondrion (Mercer et al, 2011; Smirnov et al, 2011; Antonicka et al, 2013; Jourdain et al, 2013). Numerous long non-coding RNAs and microRNAs have been localized to mitochondria, and potential functions include storage and regulation of transcription and translation (Dong et al, 2017). Given the large number of microRNAs, the microRNA subset that resides in mitochondria is referred to as miRNAs of nuclear or mitochondrial origin that are localized in mitochondria (MitomiRs) and have a wide variety of proposed functions in mitochondrial gene expression and regulation (Bandiera et al, 2013; Geiger & Dalgaard, 2017).

In addition to import, initial results in our collaborative study with the Proudfoot group have shown that loss of PNPase resulted in the export of mtDNA to the cytosol (Dhir et al, 2018). The mtDNA molecules are novel DAMPs that activate MDA5 and RIG-I and trigger the antiviral IFN-1 response pathway (Dhir et al, 2018). Exported mtDNA molecules have also been characterized in a fly model that lacks functional mitochondrial poly(A) polymerase (Pajak et al, 2019).

Although the transport mechanism of RNAs across mitochondrial membranes is not well understood, numerous studies indicate different RNA species use different translocation pathways, suggesting that RNA import pathways may have been developed independently several times during evolution (Salinas et al, 2008). A common feature for RNA import is the requirement of a membrane potential and an energy form such as ATP. The necessity of energy is in the form of ATP hydrolysis and maintenance of the mitochondrial inner membrane potential. Additional properties of RNA import mechanisms may vary based on the RNA species and the organism. Tarassov and colleagues have shown that tRNA^{Lys} import in yeast requires enolase and cytosolic precursors of aminoacyl-tRNA synthetases (Tarassov et al, 1995; Kamenski et al, 2010). Mitochondrial PNPase has been shown to act as a gatekeeper to mediate the import of a subset of RNAs into mitochondria (Wang et al, 2010; Wang et al, 2012b; Vedrenne et al, 2012).

The export mechanism of mtDNA from mitochondria highlights a new pathway in which mtDNA molecules are exported from mitochondria that maintain a membrane potential (Chen et al, 2006). A central question is how the mitochondria remain functional while the large mtDNA molecules are exported. Here, we build on our earlier collaboration (Dhir et al, 2018) and begin to outline a pathway for the export of mtDNA molecules. At the outer membrane, VDAC and BAK/BAX, which have been implicated in mtDNA release (McArthur et al, 2018; Tigano et al, 2021), are key components, whereas the inner membrane components prohibitin 1 and 2 (PHB1/PHB2) are candidates that mediate release across the inner membrane.

Results

PNPase but not SUV3 is required for the export of mtDNA molecules to the cytosol

In a previous collaborative study, BAK and BAX participated in mtDNA export (Dhir et al, 2018), akin to the release of mtDNA

during apoptosis (Rongvaux et al, 2014; White et al, 2014; McArthur et al, 2018). However, as BAK and BAX are typically associated with apoptosis and patients with PNPase mutations survive until late in life (Vedrenne et al, 2012; von Ameln et al, 2012; Eaton et al, 2018; Sato et al, 2018; Rius et al, 2019), activation of a classic apoptotic pathway is unlikely. We sought to characterize the mtDNA export pathway in detail. We used immunofluorescence microscopy with a monoclonal antibody (J2) that is specific for dsDNA and is widely used to detect viral dsDNA in plant and animal cells (Weber et al, 2006). The monoclonal J2 antibody was developed against the dsDNA killer virus of *Saccharomyces cerevisiae* and recognizes dsDNAs that are ~40–50 nucleotides or longer (Schonborn et al, 1991).

We first confirmed a linear pathway in which SUV3 knockdown (KD) followed by PNPase KD was required for release of mtDNA molecules to the cytosol (Dhir et al, 2018). An RNAi KD strategy was used instead of genomic deletion for PNPase (Fig S1A) because cells that lack PNPase lose mtDNA and become rho null (ρ^0) (Shimada et al, 2018). SUV3 was also knocked down with RNAi (Fig S1B). Previous studies have suggested that PNPase and SUV3 form a complex (Borowski et al, 2013), suggesting that their expression may be co-dependent. However, we show that PNPase and SUV3 protein levels are not dependent upon each other (Fig S1A and B), indicating that these proteins are not bona fide partners. As a negative control (Ctl), a non-targeting RNAi construct did not affect the expression of PNPase or SUV3.

We investigated the subcellular localization of mtDNA molecules when PNPase and/or SUV3 were knocked down in HeLa cells. With the non-targeting RNAi construct (Ctl), mtDNA molecules (marked by red fluorescence) were essentially not detected in mitochondria, which were marked with TOMM40 (green fluorescence) (Fig 1). SUV3 KD resulted in accumulation of mtDNA molecules in mitochondria in small puncta that overlapped with the mitochondrial marker TOMM40. However, a fraction of mtDNA molecules was detected in puncta in the cytosol when PNPase was knocked down (Fig 1). When both PNPase and SUV3 were knocked down, mtDNA molecules mostly remained in mitochondria, indicating that SUV3 is required before PNPase for mtDNA release. Pearson's correlation coefficient (PCC) in ImageJ software was used to quantify co-localization of mitochondria and mtDNA (Dunn et al, 2011). PCC values of 0.73, 0.69, and 0.55 were calculated for KD of SUV3, SUV3/PNPase, and PNPase, respectively. Portions of the images were also magnified to show localization of mtDNA molecules with respect to mitochondria. Thus, the mtDNA molecules seem to specifically show decreased co-localization with mitochondria when PNPase is knocked down.

To determine the time frame in which mtDNA molecules were released, a time-course study was done when PNPase levels were reduced by RNAi (Fig S2). Over 96 h, cells remained healthy. After ~48 h, mtDNA molecules (marked by red fluorescence) began to move out of mitochondria (marked with green fluorescence) and localize to the cytosol (PCC = 0.59), and at ~60 h, the mtDNA molecules were found in cytosolic puncta. Based on this time course, 60–72 h post-RNAi treatment (PCC = 0.56) was selected for studies to evaluate mtDNA localization. At 96 h, mtDNA molecules were in red puncta and the mitochondrial network appeared largely fragmented (PCC = 0.41). Because we have previously shown that cells without PNPase lose mtDNA, cells will not continue to grow unless adapted to glycolytic

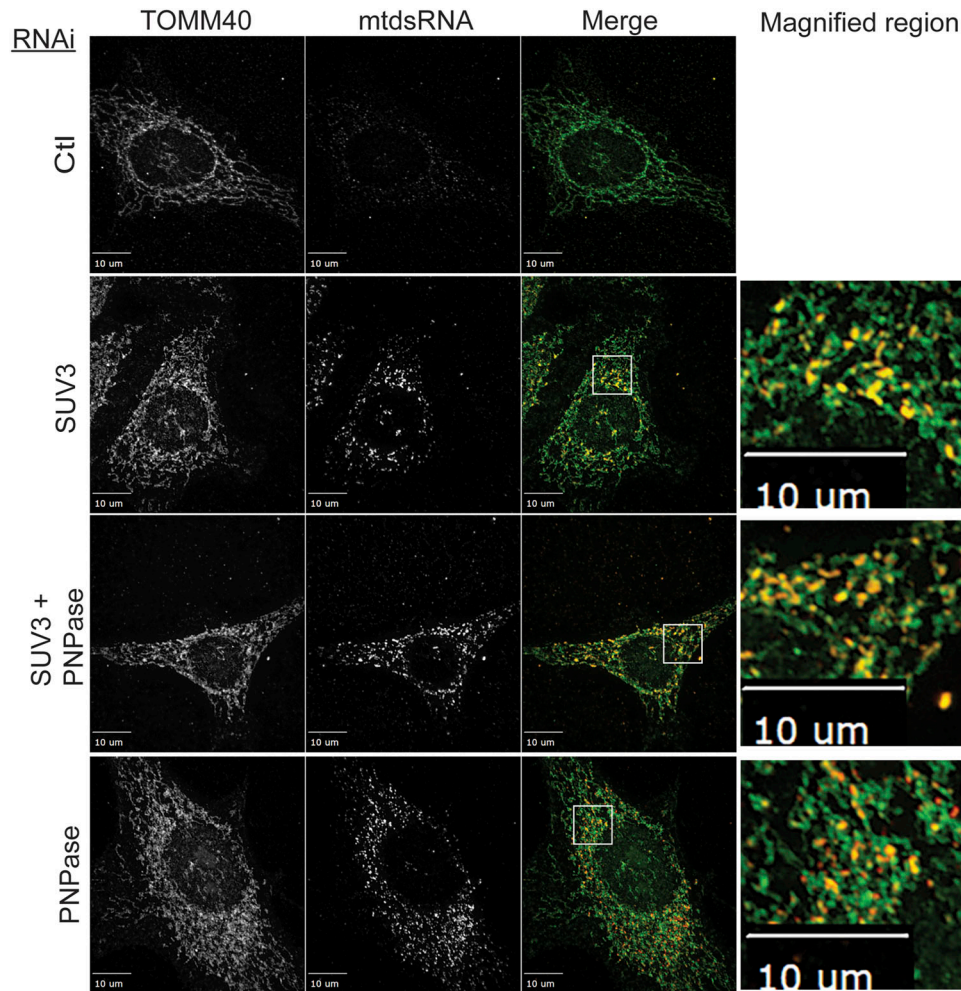


Figure 1. mtDNA accumulates in mitochondria with SUV3 KD, whereas mtDNA localizes to the cytosol with PNPase KD.

SUV3 (PCC = 0.73), PNPase (PCC = 0.55), and the combination (PCC = 0.69) were knocked down (KD) in HeLa cells with the respective RNAi construct followed by fixing on coverslips and imaging after 72 h. The mtDNA (red) was investigated by immunofluorescence with the monoclonal J2 antibody. TOMM40 was detected with a polyclonal antibody to mark mitochondria (green), and the images were merged. The right panel contains a magnified portion from the merged image (marked with a white box). As a control (Ctl), the cells were treated with a non-targeting RNAi construct. The bar indicates 10 μ m ($n = 8$).

media supplemented with uridine (Shimada et al, 2018). In summary, mtDNA was released to the cytosol in a controlled manner.

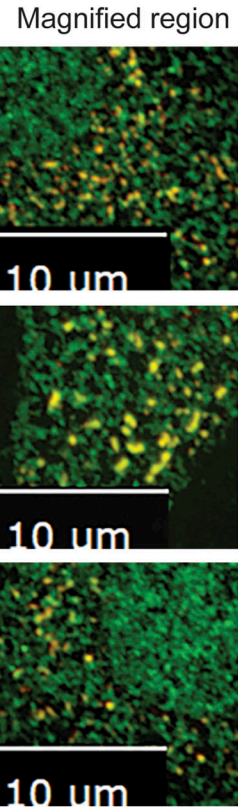
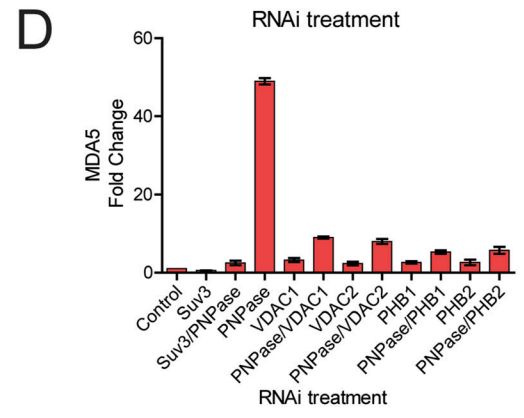
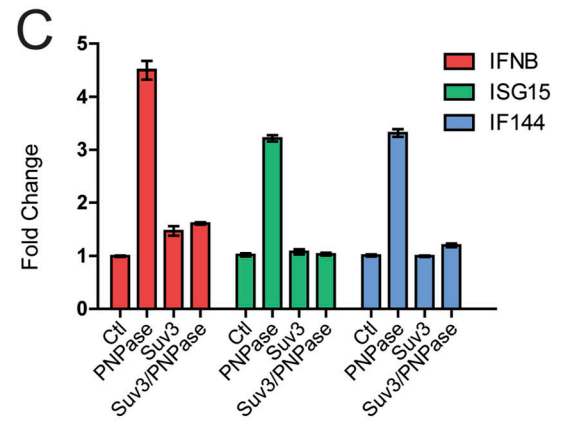
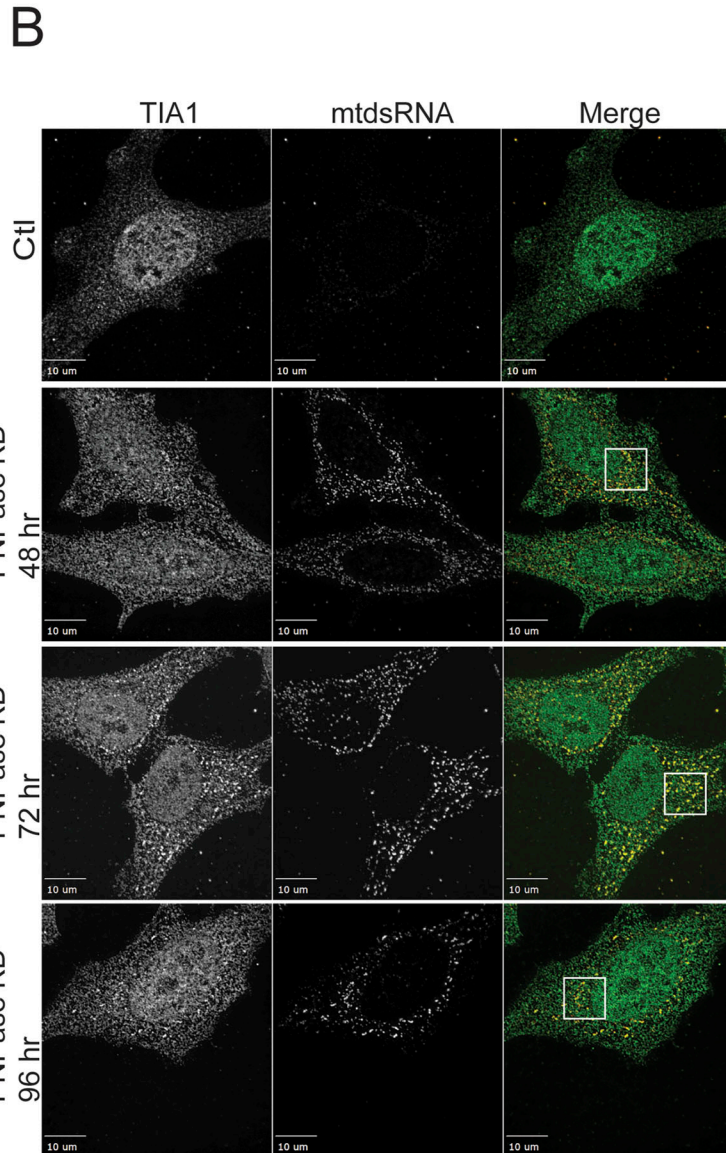
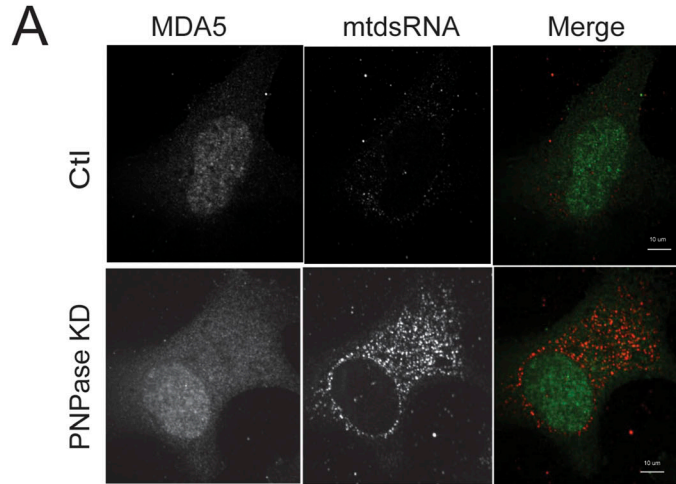
The mtDNA partially co-localize with stress granule protein TIA-1, and the type 1 IFN stress response is induced

To independently demonstrate that the dsRNAs detected above originated from mitochondria, we performed immunoprecipitation with the J2 antibody from a total cell lysate followed by Nanopore long-read sequencing. Briefly, the immunoprecipitated RNAs were polyadenylated in vitro and then sequenced using the Oxford Nanopore platform (Liu et al, 2022). After alignment with the mitochondrial genome, the RNA-sequencing profile for cells with PNPase KD showed abundant reads that mapped to both the heavy (H)- and light (L)-strands of the mitochondrial genome, implying the presence of intermolecular dsRNA (Fig S3). Most abundant mtDNA aligned to the ribosomal (r)RNAs and displacement (D)-loop regions. In addition, reads were also detected that aligned with the coding regions of the mitochondrial genome, particularly Cox1 and Cox2. For SUV3 KD, mtDNA were also detected for the rRNAs and D-loop, whereas mtDNA were barely detected for the

control cells. Because the L-strand for the rRNAs was abundant in PNPase KD, a transcript for the entire L-strand was generated from the origin of L-strand transcription.

To confirm the specificity of the dsRNAs, we also queried the sequencing reads with the nuclear genome. We only detected dsRNAs that aligned with the coding and non-coding strands for the 18S rRNA when PNPase or SUV3 was knocked down (Fig S4). Previously, dsRNAs for the 18S rRNA have not been reported, but a class of antisense ribosomal siRNAs (risRNAs) has been identified that functions in ribosomal biogenesis (Zhu et al, 2018). The dsRNA for the 18S rRNA may have a novel role in attenuating cytosolic translation during the IFN-1 response (Wan et al, 2021). In sum, the sequencing analysis confirms that the dsRNAs detected by immunofluorescence were of mitochondrial origin.

MDA5 and RIG-I are dsRNA sensors in the cytosol that recognize long (>2.0 kb) and short (<2.0 kb) dsRNAs, respectively, and relay the IFN-1 response (Kato et al, 2008; Peisley et al, 2011). Our previous study indicated that knockdown of MDA5 in PNPase-depleted cells mainly blocked the IFN-1 response, but RIG-I also did to a lesser extent (Dhir et al, 2018). We determined whether MDA5 co-localized with mtDNA in cells that were depleted for PNPase using immunofluorescence microscopy (Fig 2A). In control cells, mtDNA



was not detected and MDA5 (green) levels were low. However, PNPase KD resulted in increased MDA5 expression throughout the cell, but it failed to co-localize with mtDNA (red). It may not be surprising that MDA5 did not markedly co-localize with cytosolic mtDNAs, because published studies have noted that MDA5 did not bind to viral RNAs and the viral RNAs seemed to localize to stress granules (Langereis et al, 2013). Thus, MDA5 likely binds to mtDNAs transiently when initiating the IFN-1 response.

Given that mtDNAs are present in large structures that are reminiscent of cytosolic stress granules, we tested whether mtDNAs co-localized with the RNA binding protein TIA-1, which promotes the assembly of stress granules (Gilks et al, 2004; Asadi et al, 2021). A subset of TIA-1 (green) seemed to co-localize with mtDNAs (red) in large puncta at 72 h post-PNPase KD (Fig 2B), suggesting the mtDNAs are moved to stress granules.

The presence of mtDNAs in the cytosol mimics a viral invasion and triggers an IFN-1 response (Dhir et al, 2018). Thus, measuring the IFN-1 response is a more specific method to assess the IFN-1 response than quantitating the amount of mtDNA that localizes to the cytosol versus the mitochondria. We used qRT-PCR to quantitate the expression of a set of genes for the IFN response including *IFNB1* for IFN- β and the IFN-stimulated genes (ISGs) *IFI44* for antiviral activity and *ISG15* for signaling (Dzimiński et al, 2019). PNPase KD but not SUV3 KD resulted in the increased expression of the *IFNB1* and ISGs, indicating that the mtDNA indeed reaches the cytosol to induce the IFN-1 response (Fig 2C). Because MDA5 specifically binds to mtDNA (Dhir et al, 2018), we investigated RNA levels of *IFIH1* (gene for MDA5) with qRT-PCR 72 h after various RNAi treatments (Fig 2D). When PNPase was knocked down but not SUV3 or SUV3 and PNPase, *IFIH1* transcript levels increased markedly. Because MDA5 response with PNPase KD seemed very specific, we used *IFIH1* transcript analysis for subsequent studies. Thus, the IFN-1 pathway is specifically activated when PNPase is knocked down, confirming localization of mtDNA to the cytosol.

PNPase functions in the intermembrane space (IMS) and the matrix

Published studies report that PNPase localizes to the IMS and matrix (Chen et al, 2006; Rainey et al, 2006; Borowski et al, 2013). To determine the compartment in which PNPase functions, we replaced the endogenous mitochondrial targeting sequence (MTS), which consists of amino acids 1–37. To target to the IMS, a construct (designated IMS-PNPase) with the MTS (amino acids 1–68) from serine β -lactamase-like protein LACTB was generated (Polianskyte et al, 2009; Rhee et al, 2013). To target to the matrix, a construct (designated Mat-PNPase) with the MTS (amino acids 1–69) of *N. crassa* F₀-ATPase subunit 9 was generated (Pfanter et al, 1987). The constructs were integrated into a HeLa T-Rex

FLP-In cell line; expression was induced with 500 ng/ml doxycycline, and endogenous PNPase was simultaneously silenced (Fig S5A). Mat-PNPase and IMS-PNPase contained a C-terminal FLAG tag for detection, and the empty vector was also included as a control. Experiments in which the mitochondrial outer membrane was ruptured by incubation in hypotonic buffer but the inner membrane remained intact indicated that the constructs were targeted correctly (Fig S5B). Abundant mtDNAs (marked by red fluorescence) in the cytosol were detected upon knockdown of endogenous PNPase (Fig 3). However, induction of PNPase targeted to the matrix or IMS resulted in markedly reduced mtDNA puncta (Fig 3). Taken together, these results indicate that PNPase surprisingly functions in both the IMS and matrix.

Outer membrane components VDAC and BAK/BAX mediate transport of mtDNAs

In collaborative studies, we previously showed that BAK or BAX KD in combination with PNPase KD blocked the IFN-1 response (Dhir et al, 2018), suggesting that mtDNAs were not exported from mitochondria to the cytosol. Thus, we investigated the localization of mtDNA in the MEF cell line in which BAX and BAK were both knocked out (Bak/Bak DKO) (Takeuchi et al, 2005). RNAi constructs specific for mouse PNPase or a non-targeting RNAi construct (Ctl) were used for KD. The mtDNA (red) localization was determined by immunofluorescence, and mitochondria were marked with an antibody against TOMM40 (green) (Fig 4A). In WT MEFs, mtDNAs localized to the cytosol when PNPase was deleted (data not shown). However, in the MEFs that lacked BAK and BAX with PNPase KD, mtDNAs co-localized with mitochondria (PCC = 0.79) and were not released into large cytosolic puncta (Fig 4A). Instead, the mitochondrial morphology seems to be altered in that an enlarged mitochondrial network surrounds the mtDNA.

The BAX inhibitor peptide V5, which blocks BAX translocation to mitochondria (Gomez et al, 2007), was also used to determine whether mtDNA export was attenuated (Fig 4B). HeLa cells were treated with 100 μ M V5 peptide (Gomez et al, 2007), and PNPase was simultaneously knocked down followed by immunofluorescence microscopy. Whereas mtDNA (green) localized to the cytosol in PNPase KD (PCC = 0.50), the addition of V5 peptide resulted in mtDNA that showed increased co-localization with mitochondria (red, PCC = 0.74). Taken together, BAK and BAX are important for mtDNA localization to the cytosol.

Because VDAC mediates the import of RNAs into mitochondria, as well as the export of mtDNA from mitochondria (Kim et al, 2019), we also considered it as a candidate for mtDNA export. Of the three VDAC genes, VDAC1 is expressed most abundantly, followed by VDAC2, and finally, VDAC3 is least expressed (Yamamoto et al, 2006). VDAC2 through association with BAK inhibits apoptosis (Cheng et al,

Figure 2. Cytosolic mtDNA co-localizes with TIA-1 but not MDA5, and the type 1 IFN pathway is induced.

(A) PNPase was knocked down by RNAi in HeLa cells, and cells were fixed for immunofluorescence studies at 72 h. MDA5 (green) and mtDNA (red) were localized, and the individual images were merged. As a control (Ctl), the cells were treated with a non-targeted RNAi construct. The bar indicates 10 μ m ($n = 3$). **(A, B)** As in “(A)” except that TIA-1 (green) and mtDNA (red) at 48 (PCC = 0.58), 72 (PCC = 0.66), and 96 (PCC = 0.40) hrs were localized. As a control (Ctl), the cells were treated with a non-targeted RNAi construct. The right panel contains a magnified region from the merged image (marked with a white box). The bar indicates 10 μ m ($n = 3$). **(C)** As in Fig 1, SUV3 and PNPase RNAi constructs were applied to HeLa cells, and 72 h post-transfection, qRT-PCR analysis of *IFNB1* and *ISG15* and *IFI44* was performed. Three technical and biological replicates were analyzed. **(C, D)** As in “(C)”, qRT-PCR analysis of *IFIH1* (MDA5 protein) transcript levels was performed 72 h after the indicated RNAi treatments. Three technical and biological replicates were analyzed.

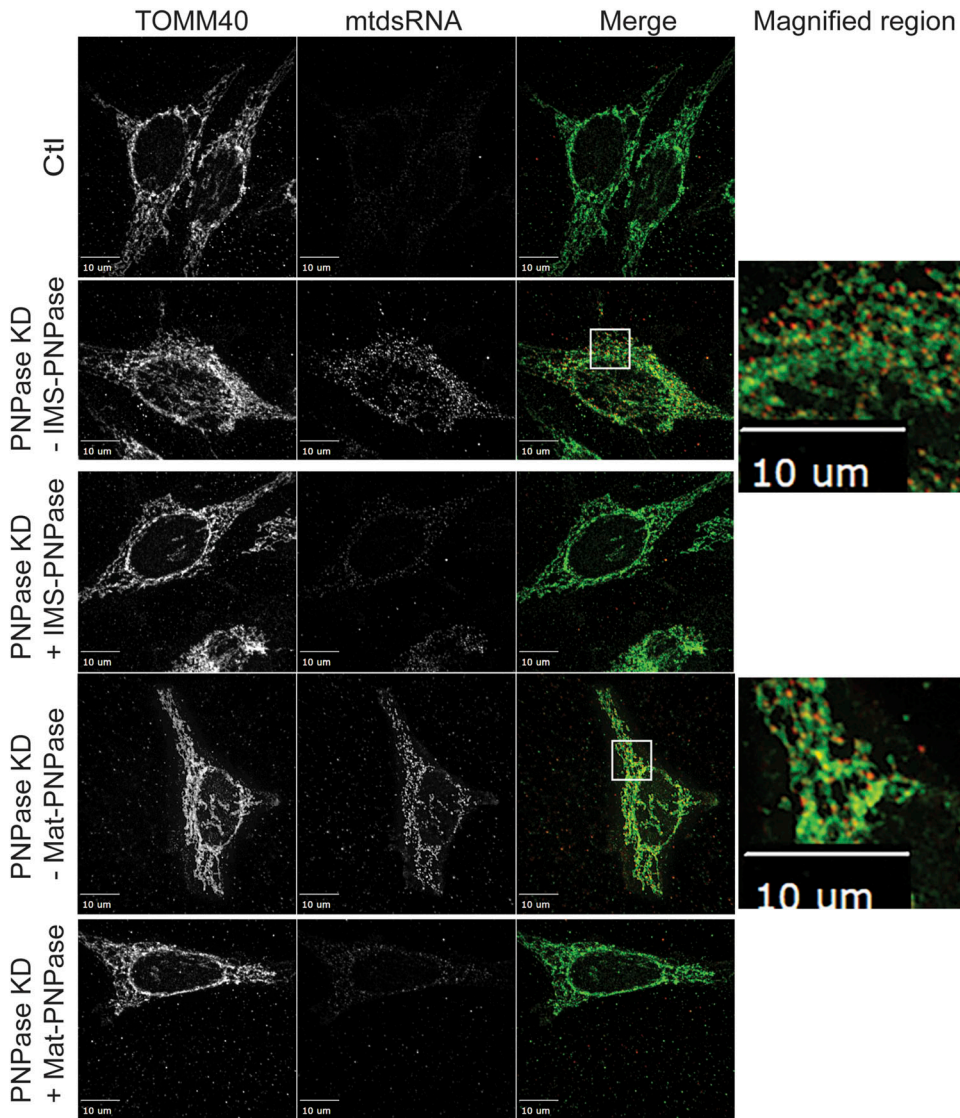


Figure 3. PNPase targeted to the IMS or matrix rescues PNPase KD.
 PNPase constructs were generated in which the native MTS was replaced with an IMS (IMS-PNPase) or matrix (Mat-PNPase) targeting sequence, and the constructs were integrated into a HeLa T-Rex Flp-In cell line; expression was induced with doxycycline. In a series of experiments, the expression of IMS-PNPase or Mat-PNPase was induced (+) with 500 ng/ml doxycycline or not induced (-) followed by PNPase KD. After 60 h, cells were fixed for imaging. The mtdsRNA (red) and mitochondria (green) were detected as in Fig 1. As a control (Ctl), the cells were treated with a scrambled RNAi construct. The bar indicates 10 μ m. The right panel contains a magnified region from the merged image (marked with a white box) for conditions in which mtdsRNA was detected ($n = 5$).

2003), suggesting the VDAC2 may have a unique function. We investigated a combination of VDAC1 or VDAC2 KD with PNPase KD (Fig 5). The mtdsRNA (green) localized to the cytosol when PNPase alone was knocked down (PCC = 0.51), but KD combinations of VDAC1 (PCC = 0.81) or VDAC2 (PCC = 0.68) with PNPase resulted in mtdsRNA that markedly co-localized with mitochondria (red). Of note, the mitochondrial network seems more fragmented with VDAC KD. MDA5 expression also was not induced markedly when by VDAC1 or VDAC2 KD alone or in combination with PNPase KD (Fig 2D), supporting that mtdsRNA was not being exported to the cytosol.

To complement the VDAC knockdown studies, we used the chemical 4,4'-diisothiocyanatostilbene-2,2'-disulfonate (DIDS) that inhibits the VDAC channel activity (Ben-Hail & Shoshan-Barmatz, 2016). DIDS is routinely used as an inhibitor for VDAC by blocking the channel and/or altering oligomerization (Ben-Hail & Shoshan-Barmatz, 2016). A titration curve with DIDS was conducted over 72 h, and a concentration of 50 μ M, which did not inhibit cell growth

or viability and was similar to the published literature (Kim et al, 2019), was selected. PNPase KD or the control RNAi construct was added to cells, and 24 h post-transfection, 50 μ M DIDS was added. At 72 h post-transfection, cells were imaged for mtdsRNA and mitochondria (Fig S6). In cells treated with DIDS that lacked PNPase, mtdsRNA (red) co-localized to mitochondria (green). In contrast, mtdsRNA showed less co-localization with mitochondria as expected when cells were not treated with DIDS. Thus, treatment with DIDS and knockdown of VDAC resulted in mtdsRNAs remaining in mitochondria. In sum, outer membrane components VDAC, BAK, and BAX seem to play a role in mtdsRNA export to the cytosol.

Prohibitin 1 and 2 are required for mtdsRNA export

The mechanism by which mtDNA or mtdsRNA crosses the mitochondrial inner membrane is not clear. Published studies suggest

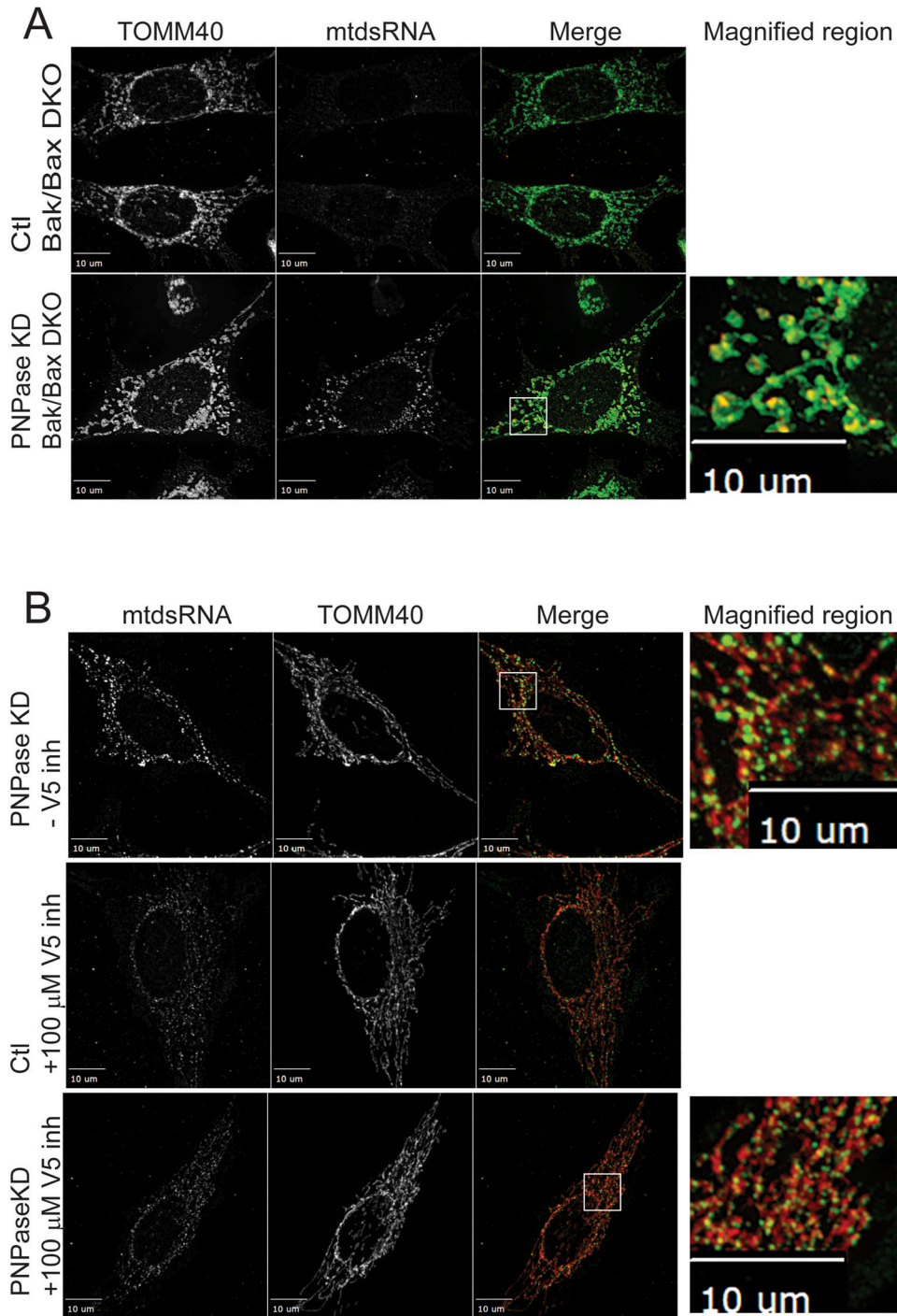


Figure 4. BAK and BAX are required for mtdsRNA release to the cytosol.

(A) BAK/BAX double-knockout MEF cell line was used for PNPase KD as in Fig 1.

Mitochondria (green) were marked with anti-TOMM40, mtdsRNA (red) was marked with anti-J2 antibody, and the images were merged. The right panel contains a magnified region from the merged image (marked with a white box) for conditions in which mtdsRNA was detected ($n = 4$).

(B) HeLa cells were treated with 100 μ M BAX inhibitor peptide V5, and PNPase was knocked down as in Fig 1. Mitochondria (green) were marked with anti-TOMM40, and mtdsRNA (red) was marked with anti-J2. The images were merged. As a control (Ctl), the cells were treated with a scrambled RNAi construct. The bar indicates 10 μ m ($n = 4$).

that mtDNA might be released by herniation of the inner membrane (McArthur et al, 2018; Riley et al, 2018) or by mitochondrial-derived vesicles (Cadete et al, 2016). Given that mitochondrial physiology was not severely compromised in a conditional mouse model that lacked PNPase in the liver (Wang et al, 2010), we reasoned that the inner membrane might have a regulated mechanism for mtdsRNA release that does not severely compromise overall mitochondrial function. In contrast, the release of mtDNA from mitochondria might be expected

to result in apoptosis, because mtDNA is essential for viability. From mass spectrometry experiments and the published literature, we considered (1) the anionic inner membrane channel CLIC5, (2) the BAK/BAX-interacting inner membrane protein GHITM, and (3) inner membrane proteins that may regulate inner membrane dynamics, prohibitin 1 and 2 (PHB1/2), as potential candidates. Although the interactions with PNPase in mass spectrometry studies were not robust (Yoshinaka et al, 2019), PHB1/2 and CLIC5 are also implicated

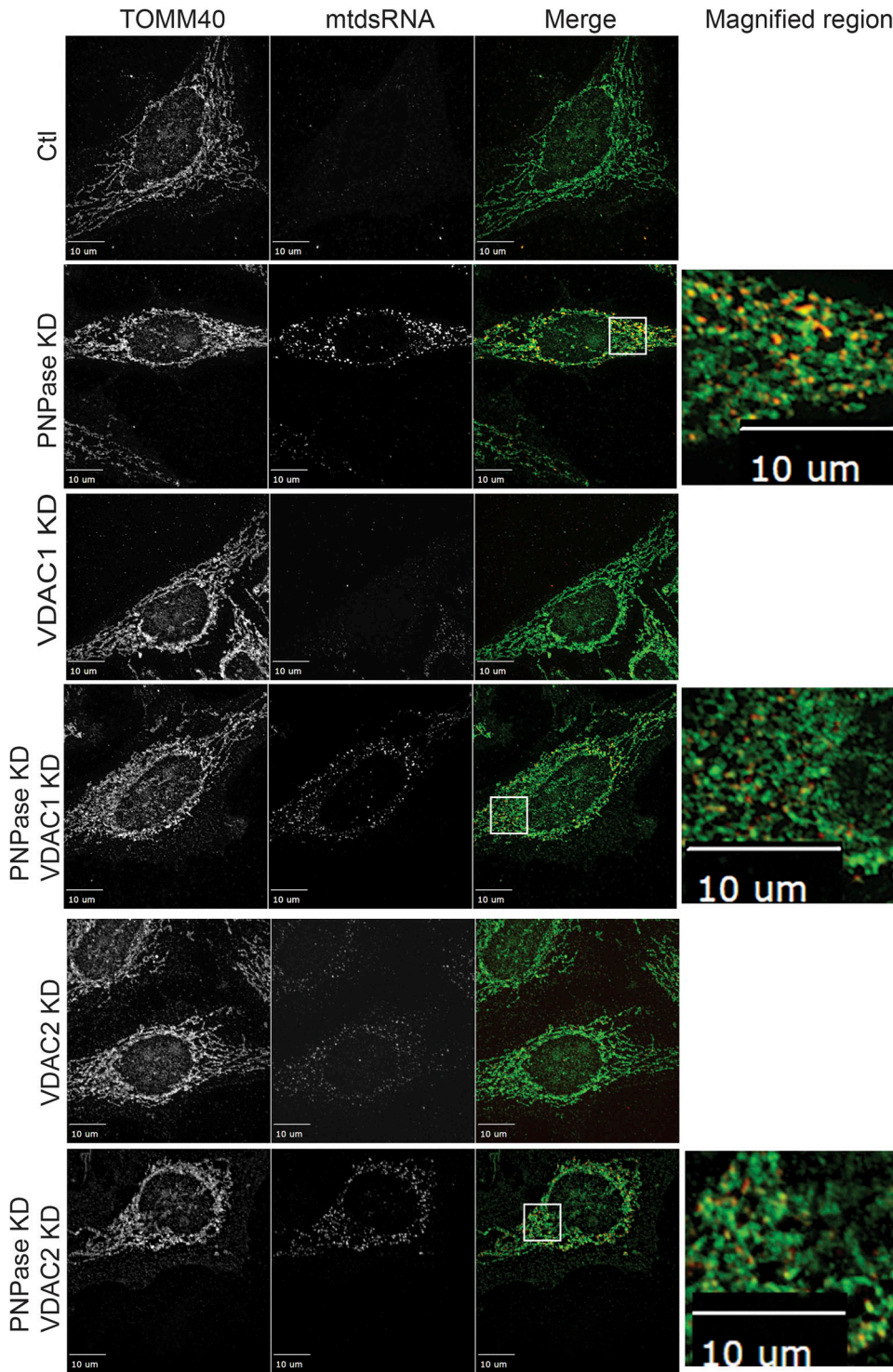


Figure 5. Knockdown or inhibition of VDAC1 or VDAC2 prevents mtdsRNA release to the cytosol.

The indicated knockdown combinations for PNPase, VDAC1, and VDAC2 were generated in HeLa cells as in Fig 1. The mtdsRNAs (green) and mitochondria (red) were detected by immunofluorescence with the J2 antibody and anti-TOMM40, respectively. The merged images are presented in the right column. The control (Ctl) is a scrambled RNAi construct. The bar indicates 10 μm ($n = 6$).

in the IFN-1 response (Langlais et al, 2016; Yoshinaka et al, 2019; Refolo et al, 2020), which is similar to PNPase. The KD of CLIC5 or GHITM in combination with PNPase KD did not block the release of mtdsRNAs (red) from mitochondria (green) (Fig S7A and B), thereby eliminating them as potential candidates. Because PHB1 and PHB2

co-assemble, the proteins were knocked down individually (Nijtmans et al, 2000; Tatsuta et al, 2005). When PHB1 (Fig 6) or PHB2 (data not shown) was knocked down singly, mtdsRNA was not detected, in contrast to KD of PNPase (PCC = 0.42). The KD of PHB1 (PCC = 0.74) or PHB2 (PCC = 0.73) in combination with PNPase KD blocked the release

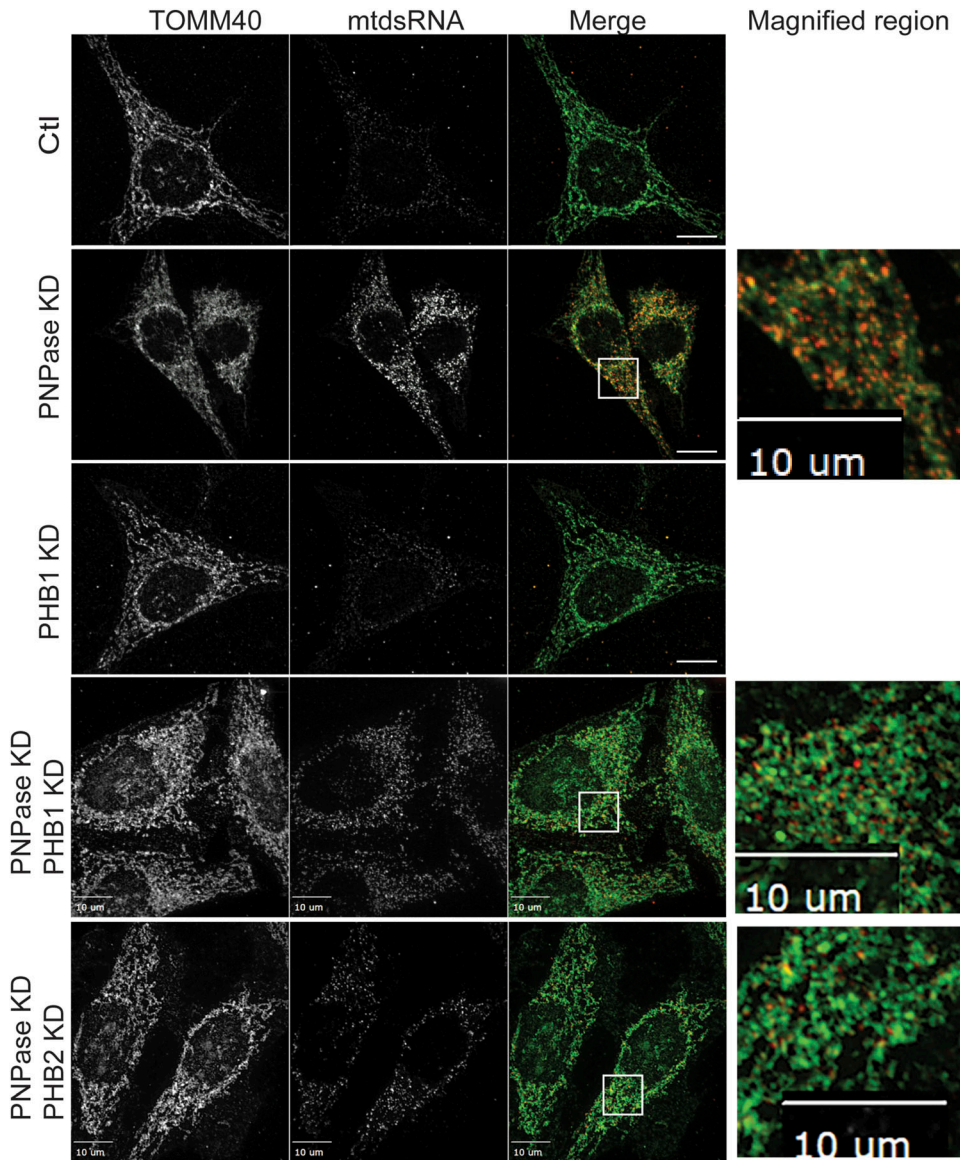


Figure 6. Knockdown or inhibition of PHB1 or PHB2 prevents mtdsRNA release to the cytosol.

The indicated knockdown combinations for PNPase, PHB1, and PHB2 were generated in HeLa cells as in Fig 1. The mtdsRNAs (red) and mitochondria (green) were detected by immunofluorescence with the J2 antibody and anti-TOMM40, respectively. The merged images are presented in the right column. The control (Ctl) is a scrambled RNAi construct for PNPase. The bar indicates 10 μm ($n = 5$).

of mtdsRNAs (red) to the cytosol, and the mtdsRNA remained in mitochondria (green) (Fig 6). In addition, the abundance of mtdsRNAs seemed to be somewhat decreased. To confirm that the mtdsRNA did not induce the IFN-1 response, MDA5 expression was not markedly elevated when PNPase was knocked down in combination with PHB1 or PHB2 (Fig 2D).

We also tested the PHB1/2 inhibitor, rocaglamide (Roc-A), which has been shown to inhibit PHB1/2 assembly (Polier et al, 2012). Roc-A was titrated over a 72-h period, and a concentration of 25–50 nM did not seem to impair cell growth. Cells were knocked down with PNPase or the control RNAi construct, and 25 nM Roc-A was added after 24 h followed by imaging at 72 h (Fig S8). The mtdsRNA (red) pool again co-localized with mitochondria (green), indicating that PHB1/2 seem to play a role in the export of mtdsRNAs to the cytosol. Thus, a candidate for release of mtdsRNAs from mitochondria is the PHB1/2 complex.

Cytosolic mtdsRNAs are detected in a subset of lung cancers

Release of mtDNAs has been reported in different cancer cell lines (Wu et al, 2021), particularly in non-small-cell lung cancer (NSCLC) cell lines where mtDNA release induces the STING signaling pathway (Kitajima et al, 2019). In addition, Roc-A treatment was shown to inhibit proliferation, migration, and anchorage-independent growth in a subset of KRAS-mutated NSCLC cell lines (Yurugi et al, 2017), suggesting mtdsRNA may be an important DAMP. In previous studies, we have characterized NSCLC cell lines and found they can be separated by preference for oxidative (OXPHOS^{HI}) versus glycolytic (OXPHOS^{LOW}) metabolism (Momcilovic et al, 2019). We reasoned that, in addition to mtDNA export, mtdsRNAs might also be exported in a subset of NSCLCs, particularly those that are glycolytic (Shimada et al, 2018). Analysis of The Cancer Genome Atlas (TCGA) database showed

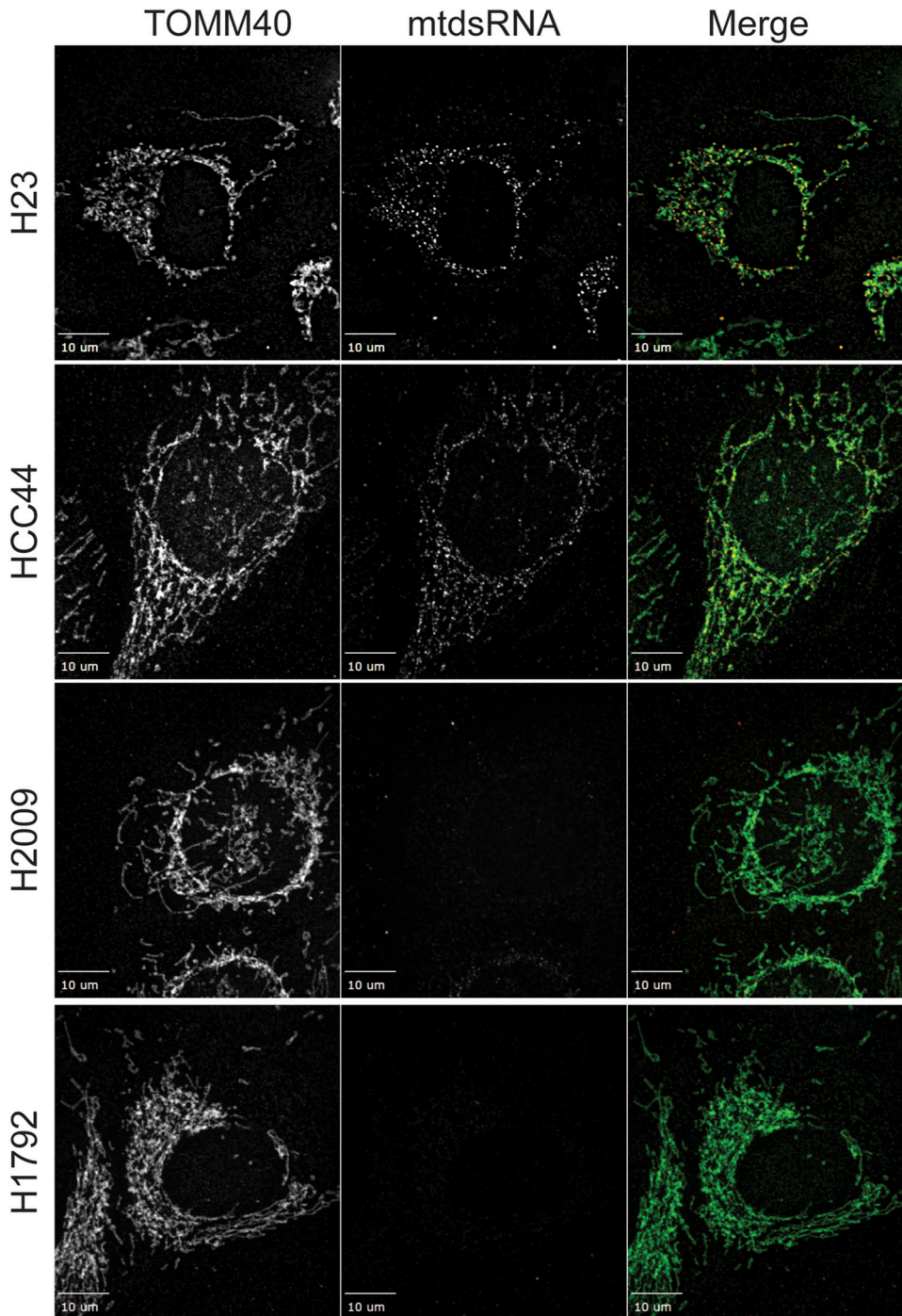
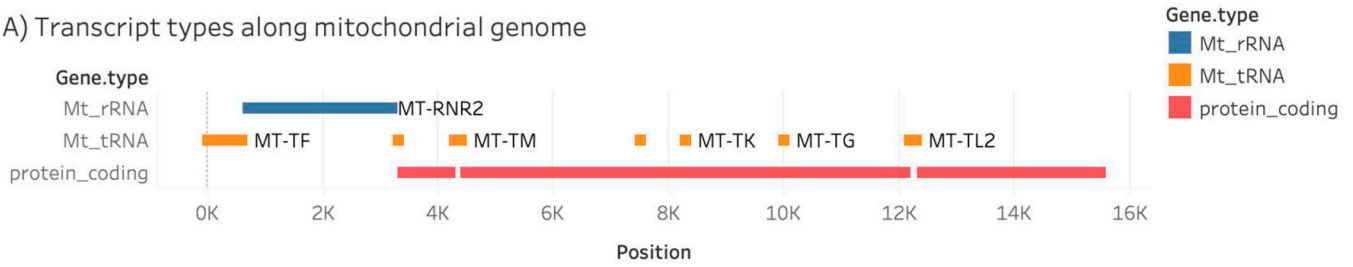


Figure 7. Subset of NSCLC cell lines have mtdsRNA localized to the cytosol. The NSCLC cell lines, H23, HCC44, H2009, and H1792, were grown on coverslips and fixed for immunofluorescence. Mitochondria (green) and mtdsRNA (red) were detected as in Fig 1. The bar indicates 10 μm ($n = 3$).

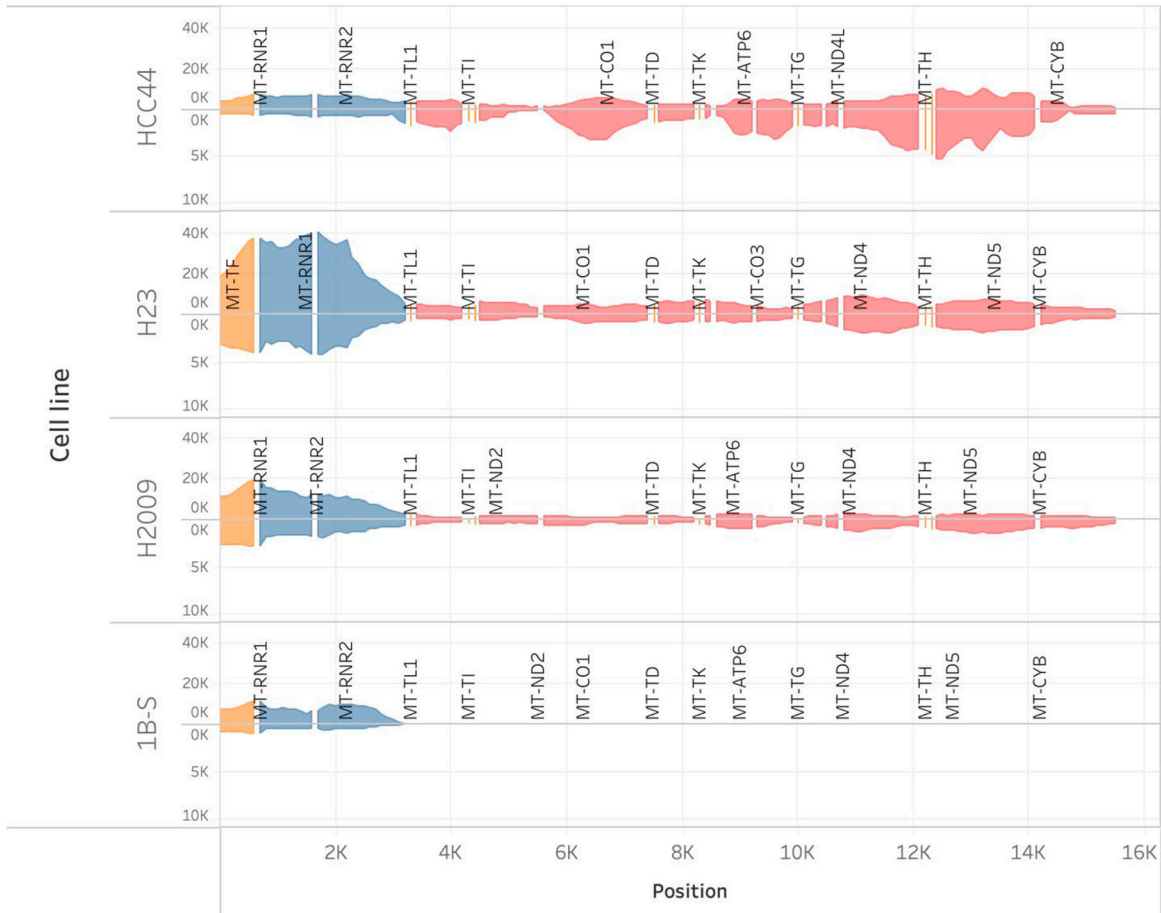
that PNPase (*PNPT1*) gene expression was up-regulated significantly in a subset of lung adenocarcinoma (LUAD) and lung squamous cell carcinoma (LUSC) lines (Fig S9) (Momcilovic et al, 2018). In addition, PNPase expression was up-regulated in numerous tumor types, compared with controls (Fig S9). Because PNPase is an IFN-1-induced gene (Leszczyniecka et al, 2003), increased PNPT1 expression in tumors may reflect those that have an increased IFN-1 response.

With well-characterized NSCLC lines, we investigated whether mtdsRNAs were detected using immunofluorescence. Barbie and colleagues previously reported in the LUAD cell line H1792 (co-mutations in *KRAS* and *TP53*, designated KP) that mtDNA was not detected in the cytosol (Kitajima et al, 2019); this cell line has an OXPHOS^{HI} metabolic profile (Chen et al, 2019). Similarly, immunofluorescence studies showed that mtdsRNAs were not detected (Fig 7). In addition, the cell line H2009, which has an OXPHOS^{HI}

A) Transcript types along mitochondrial genome



B) Distribution of recovered mitochondrial read coverages mapping to the +/- strand



Proportion of reads from dsRNA (Nucleated S1 RNased samples)

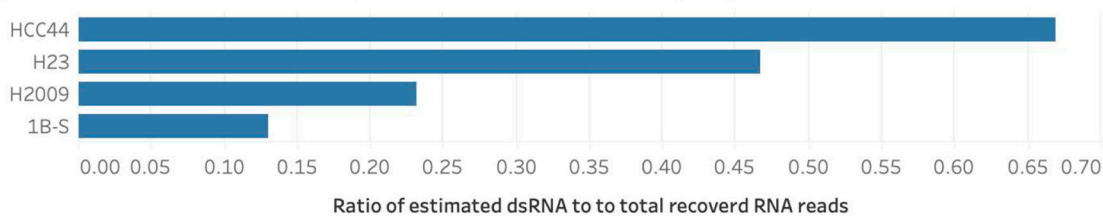


Figure 8. Sequencing of the dsRNA in H23 and HCC44 cell lines confirms that the dsRNA is from mitochondria.

RNA was purified from the H23, HCC44, and H2009 cell lines, and a negative control cell (1B-S) line, and dsRNA was prepared for sequencing. The total content and fraction of mitochondrial double-stranded reads were determined by sliding a window across the aligned read files and returning the coverage of reads mapping to the + strand for each window. **(A)** Schematic of the mitochondrial genome, including coding regions, ribosomal RNAs, and tRNAs. **(B)** Distribution of aligned reads to the mitochondrial genome. The x-axis represents mitochondrial DNA coordinates (3k to 16k). The y-axis indicates the number of reads that overlap each sliding window for

metabolic profile as well, lacked mtDNA. In contrast, abundant mtDNAs were present in LUAD cell lines, HCC44 and H23, with mutations in *KRAS* and *STK11/LKB1* (designated KL) (Fig 7). These cell lines have an OXPHOS^{LOW}, glycolytic, metabolic profile (Meijer et al, 2018; Majem et al, 2020). In the cell line H23, a cohort of the mtDNA seemed to localize to the cytosol in larger puncta when compared to the mtDNA cohort in HCC44 cells. Thus, in a subset of NSCLC cell lines, mtDNA may be exploited as a DAMP for signaling mitochondrial stress.

mtDNAs in a subset of NSCLC lines are detected by sequencing

To confirm that the dsRNAs are derived from mitochondria, we sequenced mtDNA from the NSCLC cell lines (Dhir et al, 2018). Briefly, a cell lysate was treated with DNase I to degrade DNA, then treated with S1 RNase to remove single-stranded RNA. To the remaining dsRNA, adapters were ligated followed by strand-specific RNA sequencing. The reads were aligned against the mitochondrial genome (Fig 8A). As a negative control, a cell line (1B-S) in which mtDNA was not detected by immunofluorescence was included (Fig 8B); a small amount of mitochondrial ribosomal DNA was detected, which probably formed secondary structures (Fig 8B). Similarly, a low amount of mtDNA was detected in the H2009 cell line. In contrast, a large amount of mtDNA was detected along the entire mitochondrial chromosome in the H23 and HCC44 cell lines. Interestingly, the H23 cell line has large amounts of rRNA, whereas the HCC44 cell line had greater reads in the coding region. Thus, mtDNA was most abundant in cell lines HCC44 and H23 as shown in the bottom panel (Fig 8B), confirming that mitochondria are the source of the dsRNA. Studies in NSCLC cell lines support that mtDNA may be a novel DAMP in lung cancer, supporting a physiologic role of this pathway in cancer.

Discussion

Because patients with PNPase mutations and mtDNA accumulation in the cytosol can survive until late in life (Rius et al, 2019), mitochondrial function was not strongly compromised. Indeed, a mouse model that lacks PNPase in the liver is healthy (Wang et al, 2010), but shows a 50% reduction in OXPHOS activity in the liver. This suggests that mitochondria have a physiologic pathway for mtDNA release to the cytosol. Here, we begin to outline a pathway for the export of mtDNAs from mitochondria to the cytosol where they up-regulate the IFN-1 response. The J2 antibody in combination with sequencing has been an important tool for detecting and characterizing mtDNA. Statistical measures to assess localization to the cytosol versus the mitochondrion are difficult to use in assessing whether the mtDNA has trafficked to the cytosol. Instead, the best measure for induction of the IFN-1 response seems to be the analysis of IFIH1 transcripts by qRT-PCR analysis. Because the mtDNA, upon PNPase KD, is rapidly transferred to puncta that contain TIA-1, scant amounts of mtDNA may be

required in the cytosol to induce the IFN-1 response. Surprisingly, mtDNA from SUV3 KD does not induce the IFN-1 response; perhaps the mtDNA is actively held within mitochondria. We propose that mtDNAs can be considered as a DAMP to signal mitochondrial stress in a subset of cancers and, potentially, other pathogenic states. Mechanistically, many details remain to be characterized. However, this study supports that mtDNA might be a useful marker for cancer diagnostics and the mtDNA export pathway might provide new targets for developing therapeutic strategies in treating cancer.

PNPase seems to function in both the matrix and IMS with PHB1/2

PNPase has been placed in numerous compartments. Originally, PNPase was identified as a cytosolic protein that played a role in terminal differentiation and cellular senescence (Leszczyniecka et al, 2002). However, PNPase has an N-terminal targeting sequence that directs its import into the mitochondrial IMS in a pathway that depends on Yme1 in vitro (Rainey et al, 2006). Sub-mitochondrial fractionation also showed that PNPase resided primarily in the IMS (Chen et al, 2006). Additional studies suggested that a fraction resides in the matrix and binds to SUV3 (Borowski et al, 2013), which aligns with its role in RNA degradation. Finally, PNPase has been reported to have a role in decay of cytosolic poly(A) RNAs when released during apoptosis (Liu et al, 2018), but late release of PNPase does likely not support degradation of cytosolic RNA as its primary function (Chen et al, 2006).

Given that loss of PNPase results in the export of mtDNAs to the cytosol, we took advantage of this activity to target PNPase to the IMS or matrix by appending a different targeting sequence. The IMS and matrix targeting sequences localized PNPase to the IMS or matrix, respectively. When endogenous PNPase was knocked down by RNAi in combination with the induced expression of the matrix- and IMS-forms of PNPase, the mtDNA levels were drastically reduced. These results support that PNPase seems to function in both the IMS and matrix. Mitochondrial proteins that are dual-localized to the matrix and IMS are rare. Potentially, PNPase is part of a larger export complex or channel that may contain PHB1/2, allowing PNPase to function on either side of the IM.

We used a candidate approach to determine potential components that function at the IM to release mtDNAs. Our criteria were IM proteins that had potential channel properties and induced the IFN-1 response, as well as interactions with PNPase (albeit weak). Previously, we have tried to identify partner proteins for PNPase but have not identified robust partners, and PNPase in yeast migrates in the same-sized complex as in mouse mitochondria at the inner membrane (Chen et al, 2006). Thus, PNPase seemed to lack partner proteins and may instead transiently associate with other partners.

We considered GHITM and CLIC5, but mtDNAs were exported when PNPase was knocked down. Instead, reduction of PHB1/2 by knockdown or inhibition with the small molecule inhibitor Roc-A seemed to prevent the export of mtDNAs to the cytosol. The

each of the four samples (HCC44, H23, H2009, and 1B-S). Positive and negative reads are represented, respectively, by regions above and below the baseline. The lower panel displays the estimated proportion of dsRNA reads per sample.

abundance of mtdsRNAs also seemed to be somewhat decreased. Given that PHB1/2 and PNPase expression is increased by the IFN-1 response (Yoshinaka et al, 2019), they seem to align well for export of mtdsRNA from the IM. Early cryo-EM studies showed that PHB1/2 can form a large ring (Tatsuta et al, 2005), but its structure in the mitochondrial inner membrane is not known. PHB1/2 is structurally related to the bacterial HflKC complex that binds to the AAA protease FtsH (Qiao et al, 2022). A cryo-EM structural analysis showed that 12 copies of HflK and HflC form a large cage in the membrane and four FtsH hexamers with periplasmic domains and transmembrane helices enclosed inside the cage and cytoplasmic domains situated at the base of the cage (Qiao et al, 2022). This large complex has a pore that is the size of the nascent polypeptide exit channel of the ribosome; however, given the intricacy, the complex could be dynamic in accommodating the transport of cargos such as mtdsRNA. Whether the mitochondrial AAA proteases Yme1 and Afg3L2 function with PHB1/2 in export of mtdsRNAs is not known. Interestingly, Yme1 has a role in mtDNA escape (Thorsness et al, 1993; Sprenger et al, 2021). Alternatively, the heptad repeat region of PHB2 has been suggested to form a scaffold with CLPB, ATAD3A, and AKAP1 and invoke the immune response from the mitochondrial signalosome (Yoshinaka et al, 2019). It is also likely that other proteins may participate and different pathways may exist for mtdsRNA export. A recent work by Wredenberg and colleagues showed that mtdsRNAs escape from mitochondria under conditions in which mitochondrial mRNA polyadenylation or degradation was disrupted in the fly model (Pajak et al, 2019). Finally, protein kinase RNA-activated recognizes short mtdsRNAs and can move in and out of mitochondria (Kim et al, 2018).

Mitochondrial outer membrane permeabilization is important for release of mtdsRNAs at the outer membrane

The release of mtDNA from mitochondria at the outer membrane via mitochondrial outer membrane permeabilization with subsequent activation of the cGAS/STING pathway has been well established (McArthur et al, 2018; Riley et al, 2018; Xian et al, 2022). Here, we show that VDAC and BAK/BAX also play a role in the release of mtdsRNAs. In MEF cells that are knocked out for both BAK and BAX, mtdsRNA co-localized with mitochondria. In addition, VDAC also seems to play a role. This may not be so surprising as mtDNA relies on the same proteins; however, the specific mechanism and similarities between mtDNA and mtdsRNA export are not known. A recent study suggests that the assembly rate of BAX and BAK in large channels is an important determinant of the kinetics of mtDNA release (Cosentino et al, 2022). The release of mtDNA is often associated with apoptosis (Cosentino et al, 2022); however, mtdsRNA release did not result in apoptosis, suggesting the export pathways may differ. VDAC may be an important player for differentiating between mtDNA and mtdsRNA. Alternatively, mtdsRNA may be released under low-stress conditions, with mtDNA being released under high-stress conditions when apoptosis is triggered.

In cancer, mtdsRNA as a new DAMP

A recent publication by Barbie and colleagues (Kitajima et al, 2019) dissected the underlying mechanism of immune resistance in NSCLC cell lines and found that *LKB1* loss resulted in suppression of

the IFN genes (STING) and insensitivity to cytoplasmic double-stranded DNA detection. They showed that mtDNA was released from mitochondria to the cytosol and activated STING and the innate immune response (Kitajima et al, 2019). Thus, mtDNA release from mitochondria represents an unexpected intrinsic tumor-sensing mechanism. We also find in a subset of NSCLC cell lines that mtdsRNA could be detected in LUADs characterized by an OXPHOS^{LOW}, glycolytic, metabolic profile (Shackelford & Shaw, 2009; Shackelford et al, 2013; Momcilovic et al, 2019). We confirmed that the dsRNA was derived from the mitochondria by sequencing. Indeed, most of the mitochondrial coding regions seemed to be detected, with increases in certain parts of the mitochondrial genome. In addition, the distribution of mtdsRNA in mitochondria versus cytosol seemed to differ between lung cancer cell lines with KP and KL mutations, suggesting that NSCLC cells with loss-of-function mutations in the *LKB1* (*STK11*) gene may have stronger activation of the IFN-1 pathway. Given that mtDNA release is likely associated with apoptosis and innate immune responses, mtdsRNA may represent a new marker for characterizing NSCLC types and other cancers. Moreover, this pathway might be targeted for therapeutic strategies. For example, Roc-A is a member of the flavagline family that has antitumor properties and sorafenib suppresses the both DNA- and RNA-sensing-mediated IFN-1 pathway in hepatocellular carcinoma (Huang et al, 2022). Thus, the pathway by which mtdsRNAs are generated represents a new pathway to characterize broadly in cancer. In tumors that have an IFN-1 signature, mtdsRNA may be an activator (Budhwani et al, 2018). Alternatively, in tumors that become resistant to IFN signaling through cGAS/STING (Benci et al, 2016; Jiang et al, 2020), activation of mtdsRNA release may provide a new pathway to reactivate the immune system, particularly if mtDNA release was an initial activator (Kitajima et al, 2019). Additional published studies support that mtdsRNA is detected in numerous tumors (Killarney et al, 2023).

Materials and Methods

Cell lines and culture media

HeLa (American Type Culture Collection [ATCC]), HeLa T-REx Flp-In (Life Technologies), MEF Bax Bak DKO SVO (ATCC), and NSCLC cell lines H23 (ATCC), HCC44 (DSMZ), H2009 (ATCC), and H1792 (ATCC) were maintained at 37°C in a humidified incubator with 5% CO₂. Cells were grown in high-glucose DMEM supplemented with 10% FBS, 100 U/ml penicillin, and 100 µg/ml streptomycin, with the exception of the MEF cell line that was supplemented with 5% FBS. Transfections were performed using BioT transfection reagent (Bioland) or Lipofectamine 2000 (Thermo Fisher Scientific) according to the manufacturer's instructions. All cell lines were routinely tested and confirmed to be free of mycoplasma using the MycoAlert mycoplasma detection kit (Lonza).

Chemicals

Chemicals were dissolved in DMSO, stored at -80°C, and used at the indicated concentrations. DMSO at 0.1% served as the vehicle

control. The following chemical inhibitors were used: Bax-inhibiting peptide V5 (#196810; Sigma-Aldrich), prohibitin-binding rocaglamide-A (#S7428; Selleck Chemicals), and VDAC inhibitor 2,2'-(1,2-ethenediyl) bis(5-isothiocyanato-benzenesulfonic acid) (DIDS) (#16125; Cayman Chemical).

Constructs

Constructs to target PNPase specifically to the IMS (IMS-PNPase) or matrix (Mat-PNPase) were constructed by removing the MTS (amino acids 1–37) from PNPase and replacing it with the MTS (amino acids 1–68) from serine β -lactamase-like protein LACTB (IMS) (Polianskyte et al, 2009; Rhee et al, 2013) or the MTS (amino acids 1–69) of *N. crassa* F₀-ATPase subunit 9 (Pfanner et al, 1987). IMS-PNPase and Mat-PNPase contained a C-terminal FLAG tag for detection. The constructs were cloned into pcDNA5/FRT/TO and then integrated into a HeLa T-Rex FLP-In cell line by transfecting cells with 1.8 μ g pOG44 (Life Technologies) and 0.2 μ g pcDNA5/FRT/TO IMS-PNPase or Mat-PNPase expression construct using BioT transfection reagent in a six-well plate. After 48 h, the cells were transferred to a 10-cm dish and stable cells were selected with 200 μ g/ml hygromycin B (Wako Pure Chemical Industries). Stable colonies were selected and maintained in 100 μ g/ml hygromycin B. IMS-PNPase and Mat-PNPase expression was induced with 500 ng/ml doxycycline for 48 h.

RNAi knockdown and small molecule modulators

Silencer Select siRNAs as indicated in Table S1 were used for knocking down target genes. Briefly, HeLa cells were transfected with 20 nM gene-specific Silencer Select using Polyplus jetPRIME transfection reagent, and 48–96 h post-transfection, cells were harvested for knockdown confirmation and immunofluorescence studies. The knockdowns were confirmed by Western blot analysis. Bax-inhibiting peptide V5 (100 μ M) was added simultaneously with an RNAi construct, whereas rocaglamide-A (25 nM) and DIDS (50 μ M) were added 24 h post-RNAi transfection.

Immunofluorescence

Cells were transferred to six-well plates including coverslips. After 24 h, cells were attached to coverslips and were fixed in 4% formaldehyde, then permeabilized in 0.25% Triton X-100. Subsequently, cells were blocked in 0.1% phosphate-buffered saline with 3% BSA and 0.1% Tween-20, followed by incubation with the primary antibody (Table S2) overnight. Cells were washed and incubated with the appropriate secondary antibodies for 1 h. The cells were washed and transferred to mounting media (Antifade GOLD reagent with DAPI; Thermo Fisher Scientific). A 3i Spinning Disk Confocal microscope (Marianas) consisting of CSU-X1 A1 Spinning Disk (Yokogawa) attached to a Zeiss Axio Observer 7 microscope (Zeiss) was used. Standard filter sets were used for imaging. The PCCs were calculated using the JACoP plugin on ImageJ.

Western blotting

Cells were lysed in RIPA buffer (50 mM Tris-HCl, pH 7.5, 150 mM NaCl, 1% NP-40, 0.1% SDS, 0.5% sodium deoxycholate, 1 mM EDTA, 1 mM PMSF [phenylmethylsulfonyl fluoride]) for 30 min on ice. After centrifugation at 21,000g for 10 min, the protein concentration was measured with the BCA protein assay kit (Thermo Fisher Scientific). Equal amounts of protein extracts were separated by SDS-PAGE and transferred to Immobilon PVDF membranes (Millipore). Proteins were detected with the indicated antibodies (Table S2) followed by chemiluminescence and imaged on ChemiDoc MP Imager (Bio-Rad).

Mitochondrial isolation from cultured cells

For large-scale mitochondrial isolation, cells were resuspended in homogenization buffer (20 mM Hepes, pH 7.4, 220 mM mannitol, 70 mM sucrose, 0.5 mM PMSF, 2.5 mM NaF, and 1 mM Na₃VO₄) and ruptured with 30 strokes in a Teflon-glass homogenizer. The homogenized cellular extract was centrifuged twice at 850g for 10 min to obtain the post-nuclear supernatant. Mitochondria were pelleted at 10,000g for 10 min and washed once in homogenization buffer. For small-scale mitochondrial isolation, cells were resuspended in homogenization buffer, if necessary supplemented with 10 mM NEM and 10 μ M MG132, and lysed by passing the cell mix through a 25-gauge needle 20 times with a 1-ml syringe. The extract was centrifuged twice at 770g for 5 min, and the supernatant was pelleted at 10,000g for 10 min to isolate mitochondria. The mitochondria were washed once with homogenization buffer. The yield was determined with the BCA protein assay kit after lysing the mitochondria in 0.1% SDS.

PNPT1 expression analysis in tumors

The gene expression data for PNPT1 from RNA sequencing and corresponding clinical information were retrieved from The Cancer Genome Atlas (<https://portal.gdc.cancer.gov/>). The expression of PNPT1 was analyzed as previously described (Momcilovic et al, 2018). The statistical tests were calculated using GraphPad Prism.

Immunoprecipitation of dsRNA

Cells were lysed in NP-40 lysis buffer (catalog #: J60766) for 30 min on ice. Protein A/G beads (catalog #: 88803) were incubated with J2 antibody suspended in NP-40 lysis buffer for 1 h at room temperature. The cell lysates were then incubated with the beads for 2 h at 4°C. The beads were washed with a high-salt PBS buffer (1x PBS, 0.1% Tween, 1 M NaCl) followed by two washes with a low-salt PBS buffer (1x PBS, 0.1% Tween, 0.5 M NaCl). The dsRNA from the immunoprecipitation was eluted by treating with 1 mg/ml Proteinase K (catalog #: P8044-1G) in NP-40 lysis buffer.

Sequencing of immunoprecipitated dsRNA with the Oxford Nanopore platform

The immunoprecipitated RNA with the J2 antibody was extracted with phenol-chloroform and then precipitated using ethanol.

Sequencing libraries were prepared from the remaining in vitro polyadenylated RNAs (~4 ng) using the PCR-cDNA barcoding sequencing kit from Oxford Nanopore (ONT, catalog #: SQK-PCB111.24) as per the manufacturer's instructions. Sequencing was performed using R9.4.1 Flongle cells on a MinION Mk1B device and sequenced for 24 h. Basecalling was performed using Guppy Basecaller (version 6.1.1+1f6bfa7f8). Reads were then mapped to the human mitochondrial genome (see Fig S3) using Minimap 2 (version 2.17-r941). Reads were visualized using IGV (version 2.12.3), and figures were prepared using Inkscape (version 1.1.2). Data are available as FASTQ files and aligned bam files.

dsRNA sequencing and analysis in cancer cell lines

A cell lysate was treated with DNase I to degrade DNA followed by a 1-h incubation at 37°C with Nuclease S1 RNase to remove single-stranded RNA. RNA was purified and incubated with 50% DMSO vol/vol for 1.5 h at 65°C to minimize the secondary structure, then purified with RNeasy MinElute Cleanup Kit (QIAGEN). Strand-specific NGS libraries were constructed from the remaining dsRNA using the KAPA RNA HyperPrep kit (Roche) and sequenced on the Illumina NextSeq using 2 × 100 bp paired-end reads.

The dsRNA-sequencing data were processed using nf-core/rnaseq pipeline, version 3.8 (Ewels et al, 2020), with the following options: reference genome, hg19; adapter and quality trimming, Trim Galore; alignment and quantification route, STAR>Salmon; sort and index alignments, SAMtools; duplicate read marking, Picard MarkDuplicates.

The strandCheckR package (To & Pederson, 2021) was used to quantify the proportion of reads originating from double-stranded RNA. First, a 100-bp window that slides over a bam file (window step = 20 bp) was used to determine the proportion of the genome with reads mapping to both the "+" and "-" strands for each window (i.e., symmetrically aligned reads). Windows that primarily include reads derived from single-stranded DNA (i.e., asymmetrically aligned reads) were eliminated. For each sliding window, the proportion of ± stranded reads was computed. Windows with more than 70% of reads from a single strand (e.g., 25% positive, 75% negative) were classified as having single-strand coverage. The remaining window was deemed coverage for double-strand RNA. Coverage of double-strand RNA was adjusted by total coverage per chromosome. Visualization of the coverage per mitochondrial region was performed using Tableau.

Quantitative PCR analysis for gene expression

Cells were lysed by drawing through a sterile 21-gauge needle and syringe to homogenize the cell. The RNA from the total lysate was isolated using the QIAGEN RNeasy spin column kit according to the manufacturer's instructions. RNA was reverse-transcribed into cDNA using Bio-Rad iScript cDNA Synthesis Kit (Bio-Rad) in accordance with the manufacturer's protocols. Reverse transcriptase quantitative PCR was performed with the 2x SYBR Green qRT-PCR kit (Kapa Biosystems) and analyzed with the Roche LightCycler 480 II system (Roche). qRT-PCR primers are listed in Table S3. Samples from three biological replicates were plated for three technical

replicates, and the average raw cycle threshold value across the three replicates was calculated.

Supplementary Information

Supplementary Information is available at <https://doi.org/10.26508/lsa.202302396>

Acknowledgements

The results for the analysis of *PNPT1* expression in tumors here are in whole or part based upon data generated by TCGA Research Network: <https://www.cancer.gov/tcga>. This work was supported by the National Institutes of Health awards CA208642 (to M Momcilovic, DB Shackelford, and CM Koehler), CA267721-01A1 (to M Momcilovic, DB Shackelford, and CM Koehler), GM073981 (to MA Teitell and CM Koehler), and GM61721 (to CM Koehler) and a seed grant from the Jonsson Comprehensive Cancer Center (to DB Shackelford and CM Koehler).

Author Contributions

MR Krieger: conceptualization, data curation, formal analysis, validation, investigation, methodology, and writing—original draft, review, and editing.

M Abrahamian: conceptualization, formal analysis, investigation, and methodology.

KL He: data curation, validation, investigation, and methodology.

S Atamdede: data curation, validation, and investigation.

H Hakimjavadi: data curation, formal analysis, visualization, and methodology.

M Momcilovic: conceptualization, formal analysis, investigation, visualization, methodology, and writing—review and editing.

D Ostrow: data curation, formal analysis, methodology, and writing—review and editing.

SDS Maggo: data curation, validation, methodology, and writing—review and editing.

YP Tsang: data curation, investigation, and methodology.

X Gai: data curation, supervision, investigation, methodology, and writing—review and editing.

GF Chanfreau: conceptualization, formal analysis, supervision, visualization, methodology, and writing—review and editing.

DB Shackelford: conceptualization, formal analysis, supervision, funding acquisition, visualization, project administration, and writing—review and editing.

MA Teitell: Conceptualization, supervision, funding acquisition, investigation, methodology, project administration, and writing—review and editing.

CM Koehler: conceptualization, resources, formal analysis, supervision, funding acquisition, validation, investigation, methodology, project administration, and writing—original draft, review, and editing.

Conflict of Interest Statement

The authors declare that they have no conflict of interest.

References

- Antonicka H, Sasarman F, Nishimura T, Paupe V, Shoubridge EA (2013) The mitochondrial rna-binding protein grsfl localizes to rna granules and is required for posttranscriptional mitochondrial gene expression. *Cell Metab* 17: 386–398. doi:10.1016/j.cmet.2013.02.006
- Asadi MR, Sadat Moslehian M, Sabaie H, Jalaie A, Ghafouri-Fard S, Taheri M, Rezazadeh M (2021) Stress granules and neurodegenerative disorders: A scoping review. *Front Aging Neurosci* 13: 650740. doi:10.3389/fnagi.2021.650740
- Bandiera S, Mategot R, Girard M, Demongeot J, Henrion-Caude A (2013) Mitomirs delineating the intracellular localization of micrnas at mitochondria. *Free Radic Biol Med* 64: 12–19. doi:10.1016/j.freeradbiomed.2013.06.013
- Becker T, Song J, Pfanner N (2019) Versatility of preprotein transfer from the cytosol to mitochondria. *Trends Cell Biol* 29: 534–548. doi:10.1016/j.tcb.2019.03.007
- Ben-Hail D, Shoshan-Barmatz V (2016) Vdac1-interacting anion transport inhibitors inhibit vdac1 oligomerization and apoptosis. *Biochim Biophys Acta* 1863: 1612–1623. doi:10.1016/j.bbamcr.2016.04.002
- Benci JL, Xu B, Qiu Y, Wu TJ, Dada H, Twyman-Saint Victor C, Cucolo L, Lee DSM, Pauken KE, Huang AC, et al (2016) Tumor interferon signaling regulates a multigenic resistance program to immune checkpoint blockade. *Cell* 167: 1540–1554.e12. doi:10.1016/j.cell.2016.11.022
- Borowski LS, Dziembowski A, Hejnowicz MS, Stepien PP, Szczesny RJ (2013) Human mitochondrial rna decay mediated by pnpase-hsuv3 complex takes place in distinct foci. *Nucleic Acids Res* 41: 1223–1240. doi:10.1093/nar/gks1130
- Budhwani M, Mazziere R, Dolcetti R (2018) Plasticity of type i interferon-mediated responses in cancer therapy: From anti-tumor immunity to resistance. *Front Oncol* 8: 322. doi:10.3389/fonc.2018.00322
- Cadete VJ, Deschênes S, Cuillerier A, Brisebois F, Sugiura A, Vincent A, Turnbull D, Picard M, McBride HM, Burelle Y (2016) Formation of mitochondrial-derived vesicles is an active and physiologically relevant mitochondrial quality control process in the cardiac system. *J Physiol* 594: 5343–5362. doi:10.1113/jp272703
- Chacinska A, Koehler CM, Milenkovic D, Lithgow T, Pfanner N (2009) Importing mitochondrial proteins: Machineries and mechanisms. *Cell* 138: 628–644. doi:10.1016/j.cell.2009.08.005
- Chen HW, Rainey RN, Balatoni CE, Dawson DW, Troke JJ, Wasiak S, Hong JS, McBride HM, Koehler CM, Teitell MA, et al (2006) Mammalian polynucleotide phosphorylase is an intermembrane space rnaase that maintains mitochondrial homeostasis. *Mol Cell Biol* 26: 8475–8487. doi:10.1128/mcb.01002-06
- Chen PH, Cai L, Huffman K, Yang C, Kim J, Faubert B, Borougs L, Ko B, Sudderth J, McMillan EA, et al (2019) Metabolic diversity in human non-small cell lung cancer cells. *Mol Cell* 76: 838–851.e5. doi:10.1016/j.molcel.2019.08.028
- Cheng EH, Sheiko TV, Fisher JK, Craigen WJ, Korsmeyer SJ (2003) Vdac2 inhibits bak activation and mitochondrial apoptosis. *Science* 301: 513–517. doi:10.1126/science.1083995
- Cosentino K, Hertlein V, Jenner A, Dellmann T, Gojkovic M, Peña-Blanco A, Dadsena S, Wajngarten N, Danial JSH, Thevathasan JV, et al (2022) The interplay between bax and bak tunes apoptotic pore growth to control mitochondrial-DNA-mediated inflammation. *Mol Cell* 82: 933–949.e9. doi:10.1016/j.molcel.2022.01.008
- Dhir A, Dhir S, Borowski LS, Jimenez L, Teitell M, Rotig A, Crow YJ, Rice GI, Duffy D, Tamby C, et al (2018) Mitochondrial double-stranded rna triggers antiviral signalling in humans. *Nature* 560: 238–242. doi:10.1038/s41586-018-0363-0
- Dong Y, Yoshitomi T, Hu JF, Cui J (2017) Long noncoding rnas coordinate functions between mitochondria and the nucleus. *Epigenetics Chromatin* 10: 41. doi:10.1186/s13072-017-0149-x
- Dunn KW, Kamocka MM, McDonald JH (2011) A practical guide to evaluating colocalization in biological microscopy. *Am J Physiol Cell Physiol* 300: C723–C742. doi:10.1152/ajpcell.00462.2010
- Dzimiński JV, Scholte FEM, Bergeron E, Pegan SD (2019) Isg15: It's complicated. *J Mol Biol* 431: 4203–4216. doi:10.1016/j.jmb.2019.03.013
- Eaton A, Bernier FP, Goedhart C, Caluseriu O, Lamont RE, Boycott KM, Parboosingh JS, Innes AMCare4Rare Canada Consortium, (2018) Is pnpt1-related hearing loss ever non-syndromic? Whole exome resequencing of adult siblings expands the natural history of pnpt1-related disorders. *Am J Med Genet A* 176: 2487–2493. doi:10.1002/ajmg.a.40516
- Ewels PA, Peltzer A, Fillinger S, Patel H, Alneberg J, Wilm A, Garcia MU, Di Tommaso P, Nahnsen S (2020) The nf-core framework for community-curated bioinformatics pipelines. *Nat Biotechnol* 38: 276–278. doi:10.1038/s41587-020-0439-x
- Garcia N, Chavez E (2007) Mitochondrial DNA fragments released through the permeability transition pore correspond to specific gene size. *Life Sci* 81: 1160–1166. doi:10.1016/j.lfs.2007.08.019
- Geiger J, Dalgaard LT (2017) Interplay of mitochondrial metabolism and micrnas. *Cell Mol Life Sci* 74: 631–646. doi:10.1007/s00018-016-2342-7
- Gilks N, Kedersha N, Ayodele M, Shen L, Stoecklin G, Dember LM, Anderson P (2004) Stress granule assembly is mediated by prion-like aggregation of tia-1. *Mol Biol Cell* 15: 5383–5398. doi:10.1091/mbc.e04-08-0715
- Gomez JA, Gama V, Yoshida T, Sun W, Hayes P, Leskov K, Boothman D, Matsuyama S (2007) Bax-inhibiting peptides derived from ku70 and cell-penetrating pentapeptides. *Biochem Soc Trans* 35: 797–801. doi:10.1042/bst0350797
- Hancock K, Hajduk SL (1990) The mitochondrial trnas of trypanosoma brucei are nuclear encoded. *J Biol Chem* 265: 19208–19215. doi:10.1016/s0021-9258(17)30645-2
- Huang Y, Liang W, Li K, Liao X, Chen J, Qiu X, Liu K, Qiu D, Qin Y (2022) Sorafenib suppresses the activation of type i interferon pathway induced by rlr-mavs and cgas-sting signaling. *Biochem Biophysical Res Commun* 623: 181–188. doi:10.1016/j.bbrc.2022.07.028
- Jeandard D, Smirnova A, Tarassov I, Barrey E, Smirnov A, Entelis N (2019) Import of non-coding rnas into human mitochondria: A critical review and emerging approaches. *Cells* 8: 286. doi:10.3390/cells8030286
- Jiang M, Chen P, Wang L, Li W, Chen B, Liu Y, Wang H, Zhao S, Ye L, He Y, et al (2020) Cgas-sting, an important pathway in cancer immunotherapy. *J Hematol Oncol* 13: 81. doi:10.1186/s13045-020-00916-z
- Jourdain AA, Koppen M, Wydro M, Rodley CD, Lightowlers RN, Chrzanowska-Lightowlers ZM, Martinou JC (2013) Grsfl regulates rna processing in mitochondrial rna granules. *Cell Metab* 17: 399–410. doi:10.1016/j.cmet.2013.02.005
- Kamenski P, Smirnova E, Kolesnikova O, Krasheninnikov IA, Martin RP, Entelis N, Tarassov I (2010) Trna mitochondrial import in yeast: Mapping of the import determinants in the carrier protein, the precursor of mitochondrial lysyl-trna synthetase. *Mitochondrion* 10: 284–293. doi:10.1016/j.mito.2010.01.002
- Kato H, Takeuchi O, Mikamo-Satoh E, Hirai R, Kawai T, Matsushita K, Hiiragi A, Dermody TS, Fujita T, Akira S (2008) Length-dependent recognition of double-stranded ribonucleic acids by retinoic acid-inducible gene-i and melanoma differentiation-associated gene 5. *J Exp Med* 205: 1601–1610. doi:10.1084/jem.20080091
- Kim Y, Park J, Kim S, Kim M, Kang MG, Kwak C, Kang M, Kim B, Rhee HW, Kim VN (2018) Pkr senses nuclear and mitochondrial signals by interacting with endogenous double-stranded rnas. *Mol Cell* 71: 1051–1063.e6. doi:10.1016/j.molcel.2018.07.029

- Killarney ST, Washart R, Soderquist RS, Hoj JP, Lebhar J, Lin KH, Wood KC (2023) Executioner caspases restrict mitochondrial RNA-driven Type I IFN induction during chemotherapy-induced apoptosis. *Nat Commun* 14: 1399. doi:[10.1038/s41467-023-37146-z](https://doi.org/10.1038/s41467-023-37146-z)
- Kim J, Gupta R, Blanco LP, Yang S, Shteinfer-Kuzmine A, Wang K, Zhu J, Yoon HE, Wang X, Kerkhofs M, et al (2019) Vdac oligomers form mitochondrial pores to release mtdna fragments and promote lupus-like disease. *Science* 366: 1531–1536. doi:[10.1126/science.aav4011](https://doi.org/10.1126/science.aav4011)
- Kitajima S, Ivanova E, Guo S, Yoshida R, Campisi M, Sundararaman SK, Tange S, Mitsuishi Y, Thai TC, Masuda S, et al (2019) Suppression of sting associated with lkb1 loss in kras-driven lung cancer. *Cancer Discov* 9: 34–45. doi:[10.1158/2159-8290.Cd-18-0689](https://doi.org/10.1158/2159-8290.Cd-18-0689)
- Langereis MA, Feng Q, van Kuppeveld FJ (2013) Mda5 localizes to stress granules, but this localization is not required for the induction of type i interferon. *J Virol* 87: 6314–6325. doi:[10.1128/jvi.03213-12](https://doi.org/10.1128/jvi.03213-12)
- Langlais D, Barreiro LB, Gros P (2016) The macrophage irf8/irf1 regulome is required for protection against infections and is associated with chronic inflammation. *J Exp Med* 213: 585–603. doi:[10.1084/jem.20151764](https://doi.org/10.1084/jem.20151764)
- Leszczyniecka M, Kang DC, Sarkar D, Su ZZ, Holmes M, Valerie K, Fisher PB (2002) Identification and cloning of human polynucleotide phosphorylase, hpnase old-35, in the context of terminal differentiation and cellular senescence. *Proc Natl Acad Sci U S A* 99: 16636–16641. doi:[10.1073/pnas.252643699](https://doi.org/10.1073/pnas.252643699)
- Leszczyniecka M, Su ZZ, Kang DC, Sarkar D, Fisher PB (2003) Expression regulation and genomic organization of human polynucleotide phosphorylase, hpnase(old-35), a type i interferon inducible early response gene. *Gene* 316: 143–156. doi:[10.1016/s0378-1119\(03\)00752-2](https://doi.org/10.1016/s0378-1119(03)00752-2)
- Liu X, Fu R, Pan Y, Meza-Sosa KF, Zhang Z, Lieberman J (2018) Pnpt1 release from mitochondria during apoptosis triggers decay of poly(a) rnas. *Cell* 174: 187–201.e12. doi:[10.1016/j.cell.2018.04.017](https://doi.org/10.1016/j.cell.2018.04.017)
- Liu Y, DeMario S, He K, Gibbs MR, Barr KW, Chanfreau GF (2022) Splicing inactivation generates hybrid mrna-snorna transcripts targeted by cytoplasmic rna decay. *Proc Natl Acad Sci U S A* 119: e2202473119. doi:[10.1073/pnas.2202473119](https://doi.org/10.1073/pnas.2202473119)
- Majem B, Nadal E, Munoz-Pinedo C (2020) Exploiting metabolic vulnerabilities of non small cell lung carcinoma. *Semin Cell Dev Biol* 98: 54–62. doi:[10.1016/j.semcdb.2019.06.004](https://doi.org/10.1016/j.semcdb.2019.06.004)
- McArthur K, Whitehead LW, Heddleston JM, Li L, Padman BS, Oorschot V, Geoghegan ND, Chappaz S, Davidson S, San Chin H, et al (2018) Bak/bax macropores facilitate mitochondrial herniation and mtdna efflux during apoptosis. *Science* 359: eaa06047. doi:[10.1126/science.aao6047](https://doi.org/10.1126/science.aao6047)
- Meijer TWH, Peeters WJM, Dubois LJ, van Gisbergen MW, Biemans R, Venhuizen J-H, Span PN, Bussink J (2018) Targeting glucose and glutamine metabolism combined with radiation therapy in non-small cell lung cancer. *Lung Cancer* 126: 32–40. doi:[10.1016/j.lungcan.2018.10.016](https://doi.org/10.1016/j.lungcan.2018.10.016)
- Mercer TR, Neph S, Dinger ME, Crawford J, Smith MA, Shearwood AM, Haugen E, Bracken CP, Rackham O, Stamatoyannopoulos JA, et al (2011) The human mitochondrial transcriptome. *Cell* 146: 645–658. doi:[10.1016/j.cell.2011.06.051](https://doi.org/10.1016/j.cell.2011.06.051)
- Momicilovic M, Bailey ST, Lee JT, Fishbein MC, Braas D, Go J, Graeber TG, Parlati F, Demo S, Li R, et al (2018) The gsk3 signaling axis regulates adaptive glutamine metabolism in lung squamous cell carcinoma. *Cancer Cell* 33: 905–921.e5. doi:[10.1016/j.ccell.2018.04.002](https://doi.org/10.1016/j.ccell.2018.04.002)
- Momicilovic M, Jones A, Bailey ST, Waldmann CM, Li R, Lee JT, Abdelhady G, Gomez A, Holloway T, Schmid E, et al (2019) In vivo imaging of mitochondrial membrane potential in non-small-cell lung cancer. *Nature* 575: 380–384. doi:[10.1038/s41586-019-1715-0](https://doi.org/10.1038/s41586-019-1715-0)
- Nijtmans LG, de Jong L, Artal Sanz M, Coates PJ, Berden JA, Back JW, Muijsers AO, van der Spek H, Grivell LA (2000) Prohibitins act as a membrane-bound chaperone for the stabilization of mitochondrial proteins. *Embo j* 19: 2444–2451. doi:[10.1093/emboj/19.11.2444](https://doi.org/10.1093/emboj/19.11.2444)
- Pajak A, Laine I, Clemente P, El-Fissi N, Schober FA, Maffezzini C, Calvo-Garrido J, Wibom R, Filograna R, Dhir A, et al (2019) Defects of mitochondrial rna turnover lead to the accumulation of double-stranded rna in vivo. *PLoS Genet* 15: e1008240. doi:[10.1371/journal.pgen.1008240](https://doi.org/10.1371/journal.pgen.1008240)
- Peisley A, Lin C, Wu B, Orme-Johnson M, Liu M, Walz T, Hur S (2011) Cooperative assembly and dynamic disassembly of mda5 filaments for viral dsrna recognition. *Proc Natl Acad Sci U S A* 108: 21010–21015. doi:[10.1073/pnas.1113651108](https://doi.org/10.1073/pnas.1113651108)
- Pfanner N, Hartl FU, Guiard B, Neupert W (1987) Mitochondrial precursor proteins are imported through a hydrophilic membrane environment. *Eur J Biochem* 169: 289–293. doi:[10.1111/j.1432-1033.1987.tb13610.x](https://doi.org/10.1111/j.1432-1033.1987.tb13610.x)
- Polianskyte Z, Peitsaro N, Dapkunas A, Liobikas J, Soliymani R, Lalowski M, Speer O, Seitsonen J, Butcher S, Cereghetti GM, et al (2009) Lactb is a filament-forming protein localized in mitochondria. *Proc Natl Acad Sci U S A* 106: 18960–18965. doi:[10.1073/pnas.0906734106](https://doi.org/10.1073/pnas.0906734106)
- Polier G, Neumann J, Thuaud F, Ribeiro N, Gelhaus C, Schmidt H, Giaisi M, Köhler R, Müller WW, Proksch P, et al (2012) The natural anticancer compounds rocaglamides inhibit the raf-mek-erk pathway by targeting prohibitin 1 and 2. *Chem Biol* 19: 1093–1104. doi:[10.1016/j.chembiol.2012.07.012](https://doi.org/10.1016/j.chembiol.2012.07.012)
- Qiao Z, Yokoyama T, Yan XF, Beh IT, Shi J, Basak S, Akiyama Y, Gao YG (2022) Cryo-em structure of the entire ftsh-hflkc aaa protease complex. *Cell Rep* 39: 110890. doi:[10.1016/j.celrep.2022.110890](https://doi.org/10.1016/j.celrep.2022.110890)
- Rainey RN, Glavin JD, Chen HW, French SW, Teitell MA, Koehler CM (2006) A new function in translocation for the mitochondrial i-aaa protease yme1: Import of polynucleotide phosphorylase into the intermembrane space. *Mol Cell Biol* 26: 8488–8497. doi:[10.1128/mcb.01006-06](https://doi.org/10.1128/mcb.01006-06)
- Reeves MB, Davies AA, McSharry BP, Wilkinson GW, Sinclair JH (2007) Complex i binding by a virally encoded rna regulates mitochondria-induced cell death. *Science* 316: 1345–1348. doi:[10.1126/science.1142984](https://doi.org/10.1126/science.1142984)
- Refolo G, Vescovo T, Piacentini M, Fimia GM, Ciccosanti F (2020) Mitochondrial interactome: A focus on antiviral signaling pathways. *Front Cell Dev Biol* 8: 8. doi:[10.3389/fcell.2020.00008](https://doi.org/10.3389/fcell.2020.00008)
- Rhee H-W, Zou P, Udeshi ND, Martell JD, Mootha VK, Carr SA, Ting AY (2013) Proteomic mapping of mitochondria in living cells via spatially restricted enzymatic tagging. *Science* 339: 1328–1331. doi:[10.1126/science.1230593](https://doi.org/10.1126/science.1230593)
- Riley JS, Quarato G, Cloix C, Lopez J, O'Prey J, Pearson M, Chapman J, Sesaki H, Carlin LM, Passos JF, et al (2018) Mitochondrial inner membrane permeabilisation enables mtdna release during apoptosis. *EMBO J* 37: e99238. doi:[10.15252/emboj.201899238](https://doi.org/10.15252/emboj.201899238)
- Rius R, Van Bergen NJ, Compton AG, Riley LG, Kava MP, Balasubramaniam S, Amor DJ, Fanjul-Fernandez M, Cowley MJ, Fahey MC, et al (2019) Clinical spectrum and functional consequences associated with bi-allelic pathogenic pnpt1 variants. *J Clin Med* 8: 2020. doi:[10.3390/jcm8112020](https://doi.org/10.3390/jcm8112020)
- Rongvaux A, Jackson R, Harman CC, Li T, West AP, de Zoete MR, Wu Y, Yordy B, Lakhani SA, Kuan CY, et al (2014) Apoptotic caspases prevent the induction of type i interferons by mitochondrial DNA. *Cell* 159: 1563–1577. doi:[10.1016/j.cell.2014.11.037](https://doi.org/10.1016/j.cell.2014.11.037)
- Rubio MA, Rinehart JJ, Krett B, Duvezin-Caubet S, Reichert AS, Soll D, Alfonso JD (2008) Mammalian mitochondria have the innate ability to import trnas by a mechanism distinct from protein import. *Proc Natl Acad Sci U S A* 105: 9186–9191. doi:[10.1073/pnas.0804283105](https://doi.org/10.1073/pnas.0804283105)
- Salinas T, Duchene AM, Marechal-Drouard L (2008) Recent advances in trna mitochondrial import. *Trends Biochem Sci* 33: 320–329. doi:[10.1016/j.tibs.2008.04.010](https://doi.org/10.1016/j.tibs.2008.04.010)
- Sato R, Arai-Ichinoi N, Kikuchi A, Matsuhashi T, Numata-Uematsu Y, Uematsu M, Fujii Y, Murayama K, Ohtake A, Abe T, et al (2018) Novel biallelic mutations in the pnpt1 gene encoding a mitochondrial-rna-import

- protein pnpase cause delayed myelination. *Clin Genet* 93: 242–247. doi:10.1111/cge.13068
- Schonborn J, Oberstrass J, Breyel E, Tittgen J, Schumacher J, Lukacs N (1991) Monoclonal antibodies to double-stranded rna as probes of rna structure in crude nucleic acid extracts. *Nucleic Acids Res* 19: 2993–3000. doi:10.1093/nar/19.11.2993
- Shackelford DB, Shaw RJ (2009) The lkb1-ampk pathway: Metabolism and growth control in tumour suppression. *Nat Rev Cancer* 9: 563–575. doi:10.1038/nrc2676
- Shackelford DB, Abt E, Gerken L, Vasquez DS, Seki A, Leblanc M, Wei L, Fishbein MC, Czernin J, Mischel PS, et al (2013) Lkb1 inactivation dictates therapeutic response of non-small cell lung cancer to the metabolism drug phenformin. *Cancer Cell* 23: 143–158. doi:10.1016/j.ccr.2012.12.008
- Shimada E, Ahsan FM, Nili M, Huang D, Atamdede S, TeSlaa T, Case D, Yu X, Gregory BD, Perrin BJ, et al (2018) Pnpase knockout results in mtdna loss and an altered metabolic gene expression program. *PLoS One* 13: e0200925. doi:10.1371/journal.pone.0200925
- Sieber F, Duchene AM, Marechal-Drouard L (2011) Mitochondrial rna import: From diversity of natural mechanisms to potential applications. *Int Rev Cell Mol Biol* 287: 145–190. doi:10.1016/B978-0-12-386043-9.00004-9
- Simpson L, Shaw J (1989) Rna editing and the mitochondrial cryptogenes of kinetoplastid protozoa. *Cell* 57: 355–366. doi:10.1016/0092-8674(89)90911-2
- Smirnov A, Entelis N, Martin RP, Tarassov I (2011) Biological significance of 5s rRNA import into human mitochondria: Role of ribosomal protein mrp18. *Genes Dev* 25: 1289–1305. doi:10.1101/gad.624711
- Somasundaran M, Zapp ML, Beattie LK, Pang L, Byron KS, Bassell GJ, Sullivan JL, Singer RH (1994) Localization of hiv rna in mitochondria of infected cells: Potential role in cytopathogenicity. *J Cell Biol* 126: 1353–1360. doi:10.1083/jcb.126.6.1353
- Sprenger HG, MacVicar T, Bahat A, Fiedler KU, Hermans S, Ehrentraut D, Ried K, Milenkovic D, Bonekamp N, Larsson NG, et al (2021) Cellular pyrimidine imbalance triggers mitochondrial DNA-dependent innate immunity. *Nat Metab* 3: 636–650. doi:10.1038/s42255-021-00385-9
- Takeuchi O, Fisher J, Suh H, Harada H, Malynn BA, Korsmeyer SJ (2005) Essential role of bax, bak in b cell homeostasis and prevention of autoimmune disease. *Proc Natl Acad Sci U S A* 102: 11272–11277. doi:10.1073/pnas.0504783102
- Tarassov I, Entelis N, Martin RP (1995) An intact protein translocating machinery is required for mitochondrial import of a yeast cytoplasmic trna. *J Mol Biol* 245: 315–323. doi:10.1006/jmbi.1994.0026
- Tatsuta T, Model K, Langer T (2005) Formation of membrane-bound ring complexes by prohibitins in mitochondria. *Mol Biol Cell* 16: 248–259. doi:10.1091/mbc.e04-09-0807
- Thorsness PE, White KH, Fox TD (1993) Inactivation of yme1, a member of the ftsh-sec18-pas1-cdc48 family of putative atpase-encoding genes, causes increased escape of DNA from mitochondria in *Saccharomyces cerevisiae*. *Mol Cell Biol* 13: 5418–5426. doi:10.1128/mcb.13.9.5418-5426.1993
- Tigano M, Vargas DC, Tremblay-Belzile S, Fu Y, Sfeir A (2021) Nuclear sensing of breaks in mitochondrial DNA enhances immune surveillance. *Nature* 591: 477–481. doi:10.1038/s41586-021-03269-w
- To T-H, Pederson S (2021) Strandcheckr: Calculate strandness information of a bam file. *R Package Version 1*. <https://github.com/UofABioinformaticsHub/strandcheckr>
- Vedrenne V, Gowher A, De Lonlay P, Nitschke P, Serre V, Boddaert N, Altuzarra C, Mager-Heckel AM, Chretien F, Entelis N, et al (2012) Mutation in pnp1, which encodes a polyribonucleotide nucleotidyltransferase, impairs rna import into mitochondria and causes respiratory-chain deficiency. *Am J Hum Genet* 91: 912–918. doi:10.1016/j.ajhg.2012.09.001
- von Arnell S, Wang G, Boulouiz R, Rutherford MA, Smith GM, Li Y, Pogoda HM, Nurnberg G, Stiller B, Volk AE, et al (2012) A mutation in pnp1, encoding mitochondrial-rna-import protein pnpase, causes hereditary hearing loss. *Am J Hum Genet* 91: 919–927. doi:10.1016/j.ajhg.2012.09.002
- Wan L, Juszkiewicz S, Blears D, Bajpe PK, Han Z, Faull P, Mitter R, Stewart A, Snijders AP, Hegde RS, et al (2021) Translation stress and collided ribosomes are co-activators of cgas. *Mol Cell* 81: 2808–2822.e10. doi:10.1016/j.molcel.2021.05.018
- Wang G, Chen HW, Oktay Y, Zhang J, Allen EL, Smith GM, Fan KC, Hong JS, French SW, McCaffery JM, et al (2010) Pnpase regulates rna import into mitochondria. *Cell* 142: 456–467. doi:10.1016/j.cell.2010.06.035
- Wang G, Shimada E, Koehler CM, Teitell MA (2012a) Pnpase and rna trafficking into mitochondria. *Biochim Biophys Acta* 1819: 998–1007. doi:10.1016/j.bbagr.2011.10.001
- Wang G, Shimada E, Zhang J, Hong JS, Smith GM, Teitell MA, Koehler CM (2012b) Correcting human mitochondrial mutations with targeted rna import. *Proc Natl Acad Sci U S A* 109: 4840–4845. doi:10.1073/pnas.1116792109
- Weber F, Wagner V, Rasmussen SB, Hartmann R, Paludan SR (2006) Double-stranded rna is produced by positive-strand rna viruses and DNA viruses but not in detectable amounts by negative-strand rna viruses. *J Virol* 80: 5059–5064. doi:10.1128/jvi.80.10.5059-5064.2006
- West AP, Shadel GS (2017) Mitochondrial DNA in innate immune responses and inflammatory pathology. *Nat Rev Immunol* 17: 363–375. doi:10.1038/nri.2017.21
- West AP, Khoury-Hanold W, Staron M, Tal MC, Pineda CM, Lang SM, Bestwick M, Duguay BA, Raimundo N, MacDuff DA, et al (2015) Mitochondrial DNA stress primes the antiviral innate immune response. *Nature* 520: 553–557. doi:10.1038/nature14156
- White MJ, McArthur K, Metcalf D, Lane RM, Cambier JC, Herold MJ, van Delft MF, Bedoui S, Lessene G, Ritchie ME, et al (2014) Apoptotic caspases suppress mtdna-induced sting-mediated type I IFN production. *Cell* 159: 1549–1562. doi:10.1016/j.cell.2014.11.036
- Wu KE, Fazal FM, Parker KR, Zou J, Chang HY (2020) Rna-gps predicts sars-cov-2 rna residency to host mitochondria and nucleolus. *Cell Syst* 11: 102–108.e3. doi:10.1016/j.cels.2020.06.008
- Wu Z, Sainz AG, Shadel GS (2021) Mitochondrial DNA: Cellular genotoxic stress sentinel. *Trends Biochem Sci* 46: 812–821. doi:10.1016/j.tibs.2021.05.004
- Xian H, Watari K, Sanchez-Lopez E, Offenberger J, Onyuru J, Sampath H, Ying W, Hoffman HM, Shadel GS, Karin M (2022) Oxidized DNA fragments exit mitochondria via mptp- and vDAC-dependent channels to activate NLRP3 inflammasome and interferon signaling. *Immunity* 55: 1370–1385.e8. doi:10.1016/j.immuni.2022.06.007
- Yamamoto T, Yamada A, Watanabe M, Yoshimura Y, Yamazaki N, Yoshimura Y, Yamauchi T, Kataoka M, Nagata T, Terada H, et al (2006) VDAC1, having a shorter n-terminus than vDAC2 but showing the same migration in an SDS-polyacrylamide gel, is the predominant form expressed in mitochondria of various tissues. *J Proteome Res* 5: 3336–3344. doi:10.1021/pr060291w
- Yoshinaka T, Kosako H, Yoshizumi T, Furukawa R, Hirano Y, Kuge O, Tamada T, Koshihara T (2019) Structural basis of mitochondrial scaffolds by prohibitin complexes: Insight into a role of the coiled-coil region. *iScience* 19: 1065–1078. doi:10.1016/j.isci.2019.08.056
- Yu C-H, Davidson S, Harapas CR, Hilton JB, Mlodzionski MJ, Laohamonthonkul P, Louis C, Low RRJ, Moecking J, De Nardo D, et al (2020) Tdp-43 triggers mitochondrial DNA release via mptp to activate cgas/sting in ALS. *Cell* 183: 636–649.e18. doi:10.1016/j.cell.2020.09.020
- Yurugi H, Marini F, Weber C, David K, Zhao Q, Binder H, Désaubry L, Rajalingam K (2017) Targeting prohibitins with chemical ligands inhibits kras-

mediated lung tumours. *Oncogene* 36: 4778–4789. doi:[10.1038/onc.2017.93](https://doi.org/10.1038/onc.2017.93)

Zhong Z, Umemura A, Sanchez-Lopez E, Liang S, Shalapour S, Wong J, He F, Boassa D, Perkins G, Ali SR, et al (2016) NF- κ B restricts inflammasome activation via elimination of damaged mitochondria. *Cell* 164: 896–910. doi:[10.1016/j.cell.2015.12.057](https://doi.org/10.1016/j.cell.2015.12.057)

Zhu C, Yan Q, Weng C, Hou X, Mao H, Liu D, Feng X, Guang S (2018) Erroneous ribosomal rnas promote the generation of antisense ribosomal

sirna. *Proc Natl Acad Sci U S A* 115: 10082–10087. doi:[10.1073/pnas.1800974115](https://doi.org/10.1073/pnas.1800974115)



License: This article is available under a Creative Commons License (Attribution 4.0 International, as described at <https://creativecommons.org/licenses/by/4.0/>).